# Investigation of Interaction between Extreme Waves and a Moored FPSO using FNPT and CFD Solvers

Zheng Zheng Hu[1], Shiqiang Yan[2*], Deborah Greaves[1], Tri Mai[1,3], Alison Raby[1], Qingwei Ma[2]

[1]*School of Engineering, Computing and Mathematics, University of Plymouth, Drake Circus, Plymouth, PL4 8AA, U.K.*
[2]*School of Mathematics, Computer Science and Engineering, City, University of London, London, EC1V 0HB, U.K.*
[3]*National University of Civil Engineering, 55 Giai Phong, Hai Ba Trung, Hanoi, Viet Nam*

[*] Shiqiang.Yan@city.ac.uk (corresponding author); Tel: +44 (0)20 7040 3330; Fax: +44(0)20 7040 8159

## Abstract

To assess the survivability of marine structures, numerical tools that can predict the interaction between extreme waves and structures are needed. Considering the significant nonlinearity associated with the problem, fully nonlinear models, including the fully nonlinear potential theory (FNPT) and general viscous flow theory based on the Navier-Stokes equation (NS) and Continuity equation, are necessary for a reliable prediction. Both methods have relatively higher computational cost compared to the linear or second order wave theories, which are popular in routine design practices. Although the FNPT model generally requires less computational efforts compared to the NS model, its theoretical assumption, i.e. the flow is incompressible, irrotational and inviscid, invalidates its applications to those problems with significant viscous effects and/or breaking waves. It is, therefore, necessary to conduct a comparative study on the accuracy of the FNPT in various problems to quantify its range of application. In this paper, both the Quasi Arbitrary Lagrangian Eulerian Finite Element (QALE-FEM) method based on the FNPT model and the open source Reynolds Average Navier-Stoke (RANS) based code, OpenFOAM, are used to predict the interaction between extreme waves and a moored Floating Production Storage and Offloading (FPSO) model. The extreme waves are generated using the NewWave theory and different wave steepnesses are used. The results, including the wave runup, pressure and force on the FPSO, are compared with the corresponding experimental data obtained from the ocean basin at the COAST Laboratory, University of Plymouth. Satisfactory agreement between the numerical predictions and the experimental measurements are observed. It is also concluded that the differences between the QALE-FEM results and the OpenFOAM results are mainly caused by the effectiveness of the wave generation in the corresponding simulations; the viscous effects may be considerable in the rotational motion of the FPSO when subjected to extreme waves.

*Keywords*: Wave-structure interaction, FNPT, OpenFOAM®, QALE-FEM, comparative study, FPSO, focused wave groups

## 1. Introduction

Offshore structures are designed to survive under wave loads experienced in the marine environment, which are likely to become more challenging due to rising sea levels and more frequent and increasingly severe storms. To secure the survivability of the offshore structures,

a reliable numerical simulation of the wave-structure interaction (WSI) in an extreme sea or survival condition is essential in the design process. Considering the fact that such problems are often highly nonlinear and may involve wave breaking and/or air entrainment, the linear and second-order diffraction/radiation models, which are commonly used in engineering practices (e.g. Dalzell, 1999; Tahar and Kim, 2003, Zang *et al*, 2006), or simplified models (e.g. Sphaier *et al.*, 2000; Lee and Choi, 2000), may not be sufficient to deliver a satisfactory prediction of the extreme wave loading on and the responses of the structures in a survival condition. Consequently, a Computational Fluid Dynamics (CFD) solution based on the Navier-Stokes (NS) equation and the Continuity equation may be sought to resolve small-scale physics associated with the viscous/turbulent effects, fluid compressibility and hydroelasticity, and to deal with breaking wave impact and air entrainment.

Significant effort has been devoted to developing in-house CFD codes, e.g. AMAZON-SC (Qian et al, 2006; Hu *et al*, 2009, 2010 and 2011), the SPH (Smoothed Particle Hydrodynamics, e.g. Lind *et al*, 2016), the MLPG-R (Meshless Local Petrov-Galekin method based on Rankine source solution, Rijas *et al*, 2019), or applying commercial (e.g. StarCCM+ and CFX by Westphalen *et al*, 2008, 2010) and open-source codes such as the OpenFOAM (Brown *et al*, 2014, 2015; Chen *et al*, 2014; Hu *et al*, 2014, 2016, 2017), for numerical modelling the WSIs in an extreme sea. These codes were developed for either single-phase (Lind *et al*, 2012; Zheng *et al*, 2014) or multi-phase (Chen *et al*, 2014; Hildebrandt and Sriram, 2014; Yan *et al*, 2015; Hu *et al*, 2016; Lind *et al*, 2016) flow and considered either incompressible (Yang *et al*, 2016; Yan *et al*, 2019), compressible (Yang *et al*, 2017) or partially compressible fluids, in which the air is compressible and the water incompressible (e.g. Lind *et al*, 2016). Different numerical methods, including the conventional mesh-based methods, e.g. the finite volume method (Hildebrandt and Sriram, 2014; Hu *et al*, 2016; Yang *et al.*, 2017), and the meshless methods, e.g. the SPH (Lind *et al*, 2012, 2016; Zheng *et al*, 2014) and MLPG-R (Ma, 2005; Zhou & Ma, 2010; Rijas *et al*, 2019), have been employed. There are also different techniques in tracking the free surface, such as the volume of fluid (VOF, e.g. Hu *et al*, 2016) and the level set (Yang *et al*, 2017), modeling turbulence, e.g. the Reynolds Average NS (Yang *et al*, 2016) and the Large-eddy simulation (LES, e.g. Xie, 2012, 2013, 2015; Yan *et al*, 2019), dealing with the velocity-pressure coupling, e.g. the fractional step method (Rijas *et al*, 2019) and PIMPLE/PISO (Hu *et al*, 2014, 2016, 2017) , modelling the motions of the floating bodies, e.g. the immersed boundary method (Yang *et al*, 2017) and solid body equation based on the Newton's 2$^{nd}$ law (e.g. Yang *et al*, 2016; Rijas *et al*, 2019), and discretizing the convective, divergence and Laplacian terms. Arguably, these codes have all been demonstrated to achieve promising accuracy in the literature, providing appropriate simulation parameters are used, which can be tuned against known experimental data. Comparative studies and blind tests have been carried out aiming to quantify the accuracy and reliability of CFD codes for different WSI problems, e.g. the water entry and slamming problem (Hong *et al*, 2017; Dias and Ghidaglia, 2018), the extreme wave interaction with fixed structures (Ransley *et al*, 2019; Yan *et al.*, 2015, 2019). However, such work did not result in a standard procedure or guideline leading to

reliable CFD predictions but revealed a great uncertainty over the required level of model fidelity when being applied to a wide range of WSI problems.

In the final report of a blind test on extreme wave interaction with a fixed Floating Production Storage and Offloading (FPSO) model (Ransley *et al*,2019), it is concluded that the overall accuracies of the CFD solutions vary significantly and do not show superiority over the accuracies of the models based on the fully nonlinear potential theory (FNPT) including the spectral element method (SEM, Engsig-Karup *et al*, 2016) and the Quasi Arbitrary Lagrangian Eulerian Finite Element Method (QALE-FEM, Ma *et al*, 2006, 2009, 2015; Yan *et al*, 2007, 2010a, 2019), although the FNPT, which assumes that the fluid is incompressible, irrotational and inviscid, has considerable model simplifications over the NS models. In addition to the above-mentioned SEM and QALE-FEM, the FNPT can be solved by other numerical methods, including the boundary element method (Grilli *et al*, 2001; Ning *et al*, 2008, 2009), conventional finite element method (Ma *et al*, 2001), high-order spectral method (Ducrozet *et al*, 2016) and spectral boundary integral method (Wang *et al*, 2015, 2018). The FNPT has shown a high accuracy within its range of application, e.g. modelling wave overturning and non-breaking wave interaction with large structures where the viscous effects are not significant. More importantly, Ransley *et al*. (2019) concluded that the CPU time spent by the FNPT model, especially the QALE-FEM, is at least one degree lower than the fastest NS models participating into the blind test. Nevertheless, the FNPT models cannot capture the small-scale viscous/turbulent effects, which may be significant near the structures when subjected to either a significant motion (Yan and Ma, 2007) or a slamming and breaking wave impact (Stansby, 2013) due to their theoretical assumptions. Consequently, to achieve a high robustness for modelling WSIs in extreme sea states, hybrid models combing the FNPT with NS models have been developed, adopting the principle that in the regions where the viscous/turbulent effects are significant, e.g., near the breaking waves and the structures, the time-consuming NS model is utilised to resolve small- and micro-scale physics, e.g. the vortex shedding and flow separation. In other regions, e.g. the wave propagation away from the structures, the effective FNPT models are employed. Typical examples include the coupling of the FNPT with commercial software (Yan and Ma, 2010b; Hildebrandt and Sriram, 2014), with the single-phase MLPG-R (Sriram *et al*, 2014; Yan and Ma, 2017) or SPH (Fourtakas *et al*, 2018), and with OpenFOAM (Li *et al*, 2018), which were developed based on the domain-decomposition strategy. It is worth noting that hybrid models using the velocity-decomposition strategy have also been developed to tackle the challenges in the WSIs (Edmund *et al*, 2013; Ferrant *et al*, 2003, 2008; Luquet *et al*, 2007). Higuera *et al*. (2018) recently developed a hybrid model coupling a Lagrangian model with OpenFOAM. Systematic reviews on the development of the hybrid models can be found by Sriram *et al*. (2014) and Li *et al*. (2018). The success of the hybrid models depends on the quantification of the error of the FNPT for WSI problems against experimental or reliable CFD solutions such that one can maximise the spatial and temporal domain for the FNPT within an acceptable error range to achieve highest overall robustness of the hybrid model. Nevertheless, such quantitative studies are limited in

the literature for WSI problems and previous research mainly focused on nonlinear wave propagation (e.g. Wang *et al,* 2017, 2018) or the cases with a fixed FPSO (Yan *et al,* 2019).

The other issue raised by Ransley *et al* (2019) is the reproduction of the incident waves for modelling WSIs. It is widely accepted that the realistic extreme waves cannot be represented by a regular wave. A commonly used approach is the focused wave group generated using the temporal-spatial focusing mechanism. The NewWave (Tromans *et al.,* 1991) has been shown to represent the average shape for an extreme wave profile consistent with the random process with a specified wave spectrum, such as the JONSWAP. Previous investigations using focused wave groups to model large transient events have been experimentally and numerically carried out by many researchers (e.g. Baldock *et al.,* 1996; Johannessen and Swan, 2001; Turnbull *et al.,* 2003; Walker *et al.,* 2004; Zang *et al.*,2006; Ma, 2007; Ning *et al.,* 2008,2009; Hu *et al.*, 2009,2010; Westphalen *et al.*,2014; Ransley *et al.*, 2019). In the numerical simulation, the transient wave groups are mainly generated by two approaches, i.e. using the wavemaker (e.g. Ma, 2007; Wang *et al.,* 2019) and specifying inlet boundary conditions (e.g. Jacobsen *et al.,* 2011; Higuera *et al.,* 2013; Hu *et al.,* 2011, 2014). Typically, the former requests a moving mesh algorithm in the numerical models and a relatively larger computational domain to ensure that the evanescent waves near the wavemaker do not influence the motion of the structures. The challenge of the latter mainly lies in accuracies of the pre-described spatial-temporal velocity, pressure and wave elevations at the inlet boundaries. For focusing wave groups, the most common method is to specify the velocity/pressure by using the superposition of the wave components obtained by the recorded gauge date at the inlet using the Fast Fourier Transform (FFT). This may be acceptable for waves with small steepness but is questionable for extreme wave events. Both approaches have been employed by Ransley *et al* (2019) and resulted in considerably different incident waves, thus influencing the overall accuracy of participated models. Generally speaking, a higher accuracy of the incident reproduction leads to a higher overall accuracy of the wave structure interaction.

In this paper, both OpenFOAM and QALE-FEM are used to simulate the focused wave interaction with a moored FPSO subjected to a wave-induced motion. Its aim is to shed some light on the above two issues, namely quantification of the error of the QALE-FEM due to neglecting viscous/turbulence effects, and the error of the focused wave generation and its subsequent effects on the motion responses of the moored FPSO,. This paper is organized as follows. The physical experiments are described in Section 2. In Section 3, the necessary descriptions of the mathematical models and relevant wave generation techniques are illustrated. The results are then described and discussed in Section 4. Conclusions are provided in Section 5.

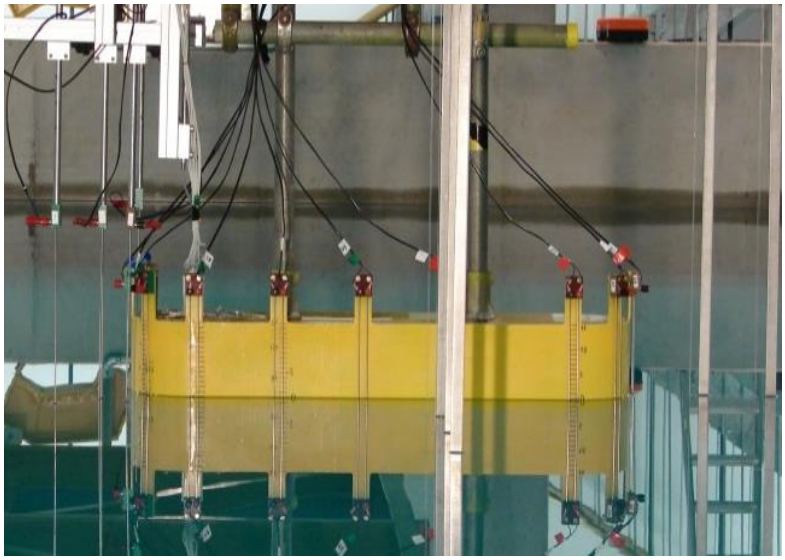

Fig.1 Simplified FPSO model with surrounding wave gauges on its surface

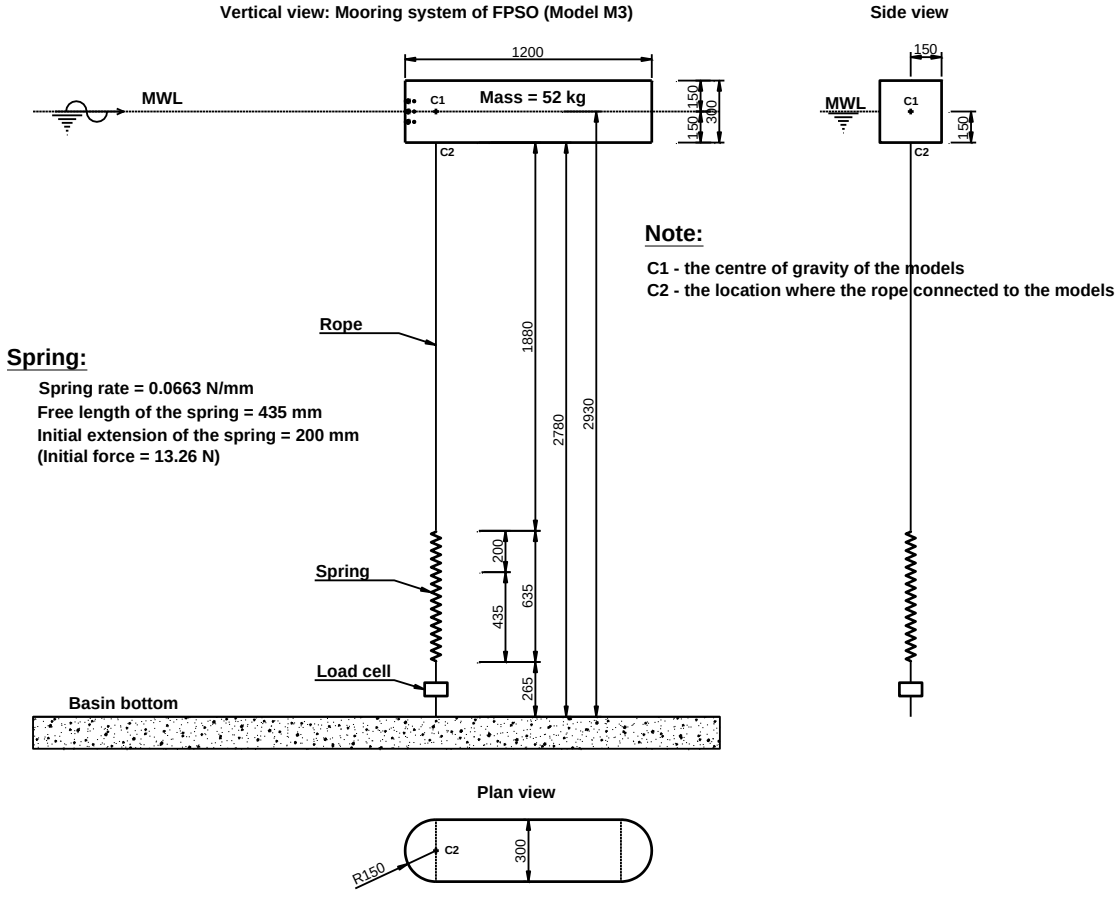


Fig.2 Illustration of the simplified FPSO model and the mooring system (unit: mm)

## 2. Physical Experiment

The experiment is carried out in the ocean basin at Plymouth University's COAST Laboratory, which is 35m long and 15.5m wide. The mean water depth in the present experiment is 2.93m. A 1/100 FPSO model with the length, breadth and depth of 1.2m, 0.3m and 0.3m respectively

is utilized in the experiment. The FPSO is simplified as a cylindrical structure with semi-circular bow and stern of 0.3m diameter and is initially placed in the water with draft of 0.15m. A photo and a sketch of the FPSO model are given in Fig. 1 and 2, respectively. A simple mooring system, consisting of a rope, spring and a load cell, is used, where the mooring point is located at 0.15m below the initial water level and attached on the bottom surface near the bow. The stiffness and the free length of the spring are 0.0663N/mm and 0.435m, respectively. The initial extension of the spring is 0.2m, yielding an initial mooring load of 13.26N. The load cell in the mooring line is located near the anchoring point C2 on the basin bed. At the rest status, the mooring line is a straight vertical line, as shown in Fig.2, and the geometric centre of the FPSO model is located at 14.486 m from the wave paddles in the plan view (i.e. the bow located at 13.886m from the wave paddles), as illustrated in Fig. 3.

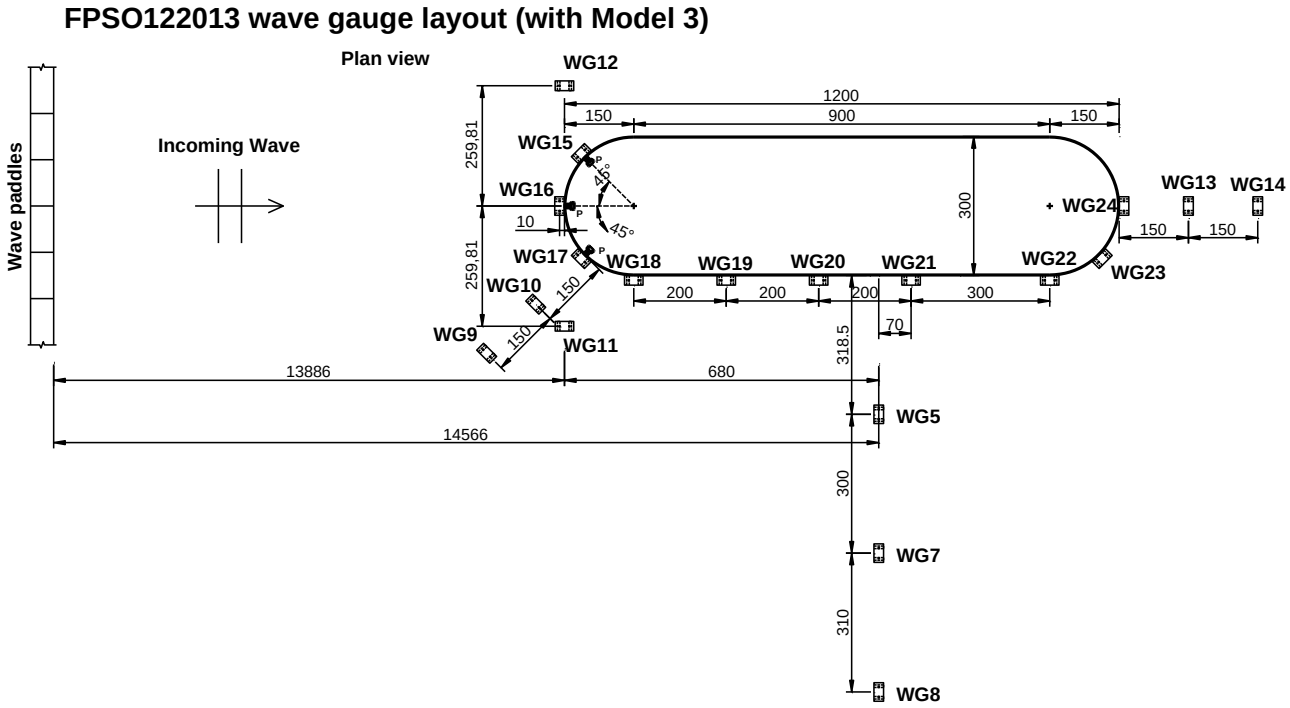


Fig.3 Position of the FPSO model and location of the wave gauges (unit: mm)

Twenty-four resistance-type wave gauges were used to measure the water elevation at various locations in the wave basin and the run-up on the FPSO surface, as illustrated in Fig. 3. The sampling frequency of the wave gauge is 128 Hz. Nine pressure sensors are installed near the bow of the FPSO surface as illustrated in Fig. 4. Pressure sensors P1, P2 and P3 on the bow are located at 0.05m above the mean water surface (MWL), in line with the MWL and 0.05m below the MWL, respectively. The vertical spacing of the sensor groups P4-P6 and P7-P9 are the same as P1-P3, but they are located at $45^o$ and $-45^o$, respectively, about the longitudinal axis of the FPSO. The sampling frequency of the pressure sensor is 1.024 kHz.

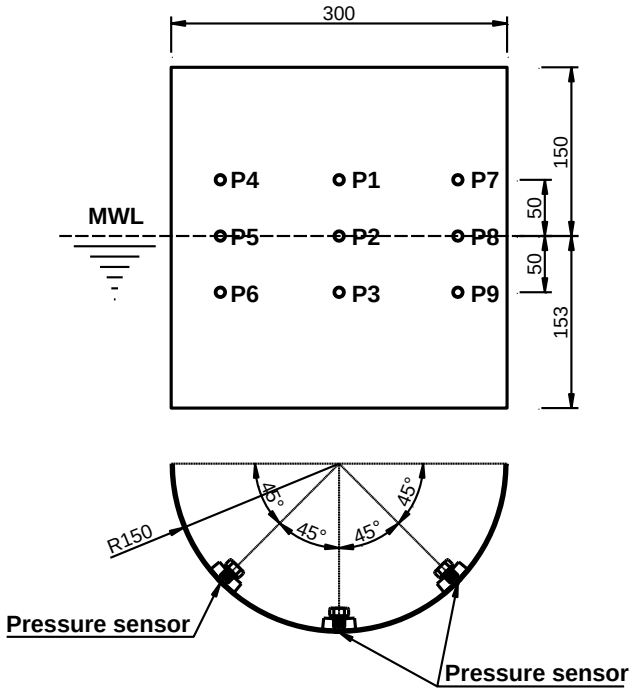


Fig.4 Location of the pressure sensors

The focusing waves are generated by the flap wave paddles with 2m hinge depth using the NewWave and spatial-temporal focusing mechanism. The characteristics of the wave conditions considered in this paper are summarized in Table 1. These waves are uni-directional and have the same peak wave period, $T_p$, but different significant wave height, $H_s$, yielding different wave steepness. The phases of the wave component are carefully tuned using an iterative procedure (see, for example, Fernández *et al*, 2013) to secure that the actual wave focusing occurs at 13.886m downstream of the wave paddle, in line with the bow of the FPSO at rest status.

Tab. 1 Characteristic waves

| Wave components | Wave period $T_p$ (s) | Wave length $\lambda_p$ (m) | Wave height *Hs* (*m*) | Frequency Band (Hz) |
|---|---|---|---|---|
| 244 | 1.456 | 3.31 | 0.077 | 0.154-2.0 |
| 244 | 1.456 | 3.31 | 0.103 | 0.1-2.0 |

## 3. Numerical Models and Wave Generation Techniques

As indicated in the Introduction, both the OpenFOAM and the QALE-FEM are used in this paper. Details of these models can be found in the papers cited and brief summaries are given here for completeness. For both models, the coordinate system (*oxyz*) is used with its origin at the mean free surface, *z*-axis pointing upward and *x*-axis pointing from the wavemaker at the left of the computational domain.

### 3.1 OpenFOAM

The two-phase incompressible Reynolds Average Navier Stokes (RANS) solver, interDyMFoam, within the OpenFOAM package is utilised in this work. In this solver, the volume of fluid (VOF) method is employed to identify air and water phases using the volume fraction, $\alpha$, the finite volume method is used to discretise the following governing equations (Jasak, 2009),

$$\frac{\partial \rho}{\partial t} + \nabla \cdot \rho \vec{u} = 0 \tag{1}$$

$$\frac{\partial \rho \vec{u}}{\partial t} + \nabla \cdot \left[\rho\left(\vec{u} - \vec{u}_g\right)\vec{u}\right] = -\nabla p - \rho \vec{g} + \nabla \cdot \left(\mu_{eff} \nabla \vec{u}\right) + \nabla \vec{u} \cdot \nabla \mu_{eff} + \sigma \kappa \nabla \alpha \tag{2}$$

$$\frac{\partial \alpha}{\partial t} + \nabla \cdot \alpha\left(\vec{u} - \vec{u}_g\right) + \nabla \cdot \vec{u}_c \alpha(1 - \alpha) = 0 \tag{3}$$

where $\vec{u}$ is the fluid velocity, $\vec{u}_g$ is the velocity of the computational grid, $\rho$ the density, $t$ the time, $p$ the pseudo dynamic pressure, $\vec{g}$ the acceleration due to gravity, $\vec{r}$ the position vector. $\mu_{eff}$ in the momentum equation (Eq. 2) is the effective dynamic viscosity and $\mu_{eff} = \mu + \rho\gamma_{turb}$, where $\mu$ is the molecular dynamic viscosity and $\nu_{turb}$ is the turbulent kinematic viscosity determined by the selected turbulence model. Here, the classic the $k - \varepsilon$ model is utilised and $\gamma_{turb} = C_d k^2/\varepsilon$, where $k$ is turbulent kinetic energy, $\varepsilon$ is turbulent eddy dissipation and $C_d$= 0.09 as recommend by Rodi (1980). The last term of Eq. (2), $\sigma\kappa\nabla\alpha$, represents the effect of surface tension, where $\sigma$ is the surface tension coefficient, $\kappa = \nabla \cdot (\frac{\nabla \alpha}{|\nabla \alpha|})$ is the curvature of the interface. The volume fraction $\alpha$ ranges from 0 to 1 and is defined as the quantity of water per unit of volume at each cell. Consequently, the density $\rho$ of the air/water mixture can be found using $\rho = \rho_{water}\alpha + \rho_{air}(1 - \alpha)$ , where subscripts 'water' and 'air' correspond to the values of the water phase and air phase respectively. Using a similar approach, the viscosity of the mixture can be determined. The volume faction is governed by the corresponding transport equation, i.e. Eq. (3), where $\nabla \cdot \vec{u}_c \alpha(1 - \alpha)$ is an artificial compressibility term (see, Weller, 2002; Rusche, 2002). The pressure-velocity coupling is solved using the PIMPLE algorithm, which originated by merging PISO (Pressure Implicit with Splitting of Operators) and SIMPLE (Semi-Implicit Method for Pressure-Linked Equations) algorithms. The solution of Eq. (3) has to be bounded between 0 and 1, by the solver MULES (Multidimensional Universal Limiter for Explicit Solution) which uses a limiter function on the fluxes of the discretised divergence term to fulfil these restrictions.

After the velocity and pressure fields are solved using Eqs. (1-3), the forces and the moment acting on the floating body due to the fluid are estimated by integrating the pressure and viscous stress over the body surface. By adding the weight, the forces/moments due to the mooring line, the total force/moment can be obtained. The translational and rotational motion of the floating body can be obtained by using Newton's 2nd law (Schwarz, 2007). In OpenFOAM, a generic sixDoFRigidBodyMotion Solver is included for solving 6DOF (six-degree-of-freedom)

motions of a rigid body (Xing *et al.*, 2008) and incorporated with the dynamic mesh technique, in which the mesh near the body is moved following the motion of the body, yielding different $\vec{u}_g$ at different computational nodes/cells (Jasak, 2007).

### 3.2 QALE-FEM

In the QALE-FEM method, the governing equation is written in terms of the velocity potential $\phi$ (Ma *et al.*, 2015; Li *et al.*, 2018) as,

$$\nabla^2\phi = 0 \tag{4}$$

On the free surface, both the kinematic and dynamic conditions read

$$\frac{D\vec{r}}{Dt} = \nabla\phi \tag{5a}$$

$$\frac{D\phi}{Dt} = -gz + \frac{1}{2}|\nabla\phi|^2 \tag{5b}$$

where D/Dt is the total time derivative following the motion of the fluid particle. On the body surface and the wavemaker,

$$\frac{\partial\phi}{\partial n} = \vec{n}\cdot\vec{U} \tag{6}$$

where $\vec{U}$ and $\vec{n}$ are the velocity and the outward unit normal vector of the rigid boundaries. On the seabed, $\frac{\partial\phi}{\partial n} = 0$. The pressure is calculated by using Bernoulli's equation,

$$p = -\rho\frac{\partial\phi}{\partial t} - \rho\frac{|\vec{\nabla}\phi|^2}{2} - \rho gz \tag{7}$$

which requires the estimation of $\frac{\partial\phi}{\partial t}$ This may be obtained using the backward finite difference scheme, which may lead to a numerical instability (Yan and Ma, 2007). To overcome this, in QALE-FEM, $\frac{\partial\phi}{\partial t}$ is evaluated by solving a similar boundary value problem, where the Laplace's equation of $\frac{\partial\phi}{\partial t}$ is used to govern the fluid motion. The boundary condition on the free surface is consistent with Eq. (5b), i.e.

$$\frac{\partial\phi}{\partial t} = -gz - \frac{1}{2}|\nabla\phi|^2 \tag{8}$$

and the boundary condition on the rigid body surface is written as,

$$\frac{\partial}{\partial n}\frac{\partial\phi}{\partial t} = \left[\vec{U}_c + \vec{\Omega}\times r\right]\cdot\vec{n} - \left(\vec{\Omega}\times\vec{U}_c\right)\cdot\vec{n} - \frac{\partial}{\partial n}\left[\left(\vec{U}_c + \vec{\Omega}\times r\right)\cdot\nabla\phi\right], \tag{9}$$

where $\vec{U}_c$ and $\dot{\vec{U}}_c$ are translational velocity and acceleration of its gravitational centre (rotational centre); $\vec{\Omega}$ and $\dot{\vec{\Omega}}$ are its angular velocity and acceleration. After the pressure on the body surface is estimated using Eq. (7), the force due to the fluid can be evaluated by integrating the pressure. In the QALE-FEM, the motion of the floating body is governed by Newton's 2nd law in the body-fixed coordinate system,

$$[M]\dot{\vec{U}}_c + [b_t]\vec{U}_c = \vec{F} \tag{10a}$$

$$[I]\dot{\vec{\Omega}} + \vec{\Omega} \times [I]\vec{\Omega} + [b_r]\vec{\Omega} = \vec{M} \tag{10b}$$

$$\frac{d\vec{S}}{dt} = \vec{U}_c \tag{10c}$$

$$[B]\frac{d\boldsymbol{\theta}}{dt} = \vec{\Omega} \tag{10d}$$

where $\vec{F}$ and $\vec{M}$ are the external forces and moments acting on the floating body in the body fixed coordinate system, considering the pressure force/moment, the weight and the mooring force/moment; $\boldsymbol{\theta}(\alpha, \beta, \gamma)$ are the Euler angles and $\vec{S}$ is the translational displacement. In Eq. (10), $[M]$ and $[I]$ are the mass and inertia-moment matrix, respectively; $[B]$ is the transformation matrix formed by Euler angles and defined as

$$[B] = \begin{bmatrix} cos\beta cos\gamma & sin\gamma & 0 \\ -cos\beta sin\gamma & cos\gamma & 0 \\ sin\beta & 0 & 1 \end{bmatrix} \tag{11}$$

$[b_t]$ and $[b_r]$ are the artificial damping coefficient representing the viscous effects on the motion of the floating body. A calibration is required in practices to $[b_t]$ and $[b_r]$ by comparing the numerical and experimental results, e.g. of the free decay test. For the problem when the motion is significant, e.g. in the resonant area, an artificial damping of 2.8% of the critical damping may be needed (Yan and Ma, 2007). The boundary value problems defined by Eqs (5-9) are solved by using a time-marching approach. The main differences between the QALE-FEM method and the conventional FEM method (Ma *et al*, 2001) is that the computational mesh is moving during the calculation by using a novel methodology based on the spring analogy method but purpose-developed for wave-structure interaction problems. In addition, this method is also equipped with three other purpose-developed techniques necessary for modelling floating structure motions in large waves: (1) a three-point method for computing the velocity on the free surfaces and body surfaces suitable for unstructured/moving meshes; (2) the modified semi-implicit time integration method for floating bodies (ISITIMFB-M), with which the difficulty associated with wave-body coupling is solved; and (3) special technique for coping with wave overturning and impacting. The details of the QALE-FEM are described by Ma & Yan (2006, 2009) and Yan & Ma (2007, 2010).

### 3.3 Wave Generation and Absorption

Wave generation is critical for accurately modelling the WSI problems in coastal and offshore engineering. As indicated in the Introduction, there are typically two approaches in the numerical practices.

The first one is to use the wavemaker and is adopted by the QALE-FEM in this paper. Considering the strong nonlinearity associated with the incoming wave, second-order wavemaker theory (Schaffer, 1996; Fernández *et al*, 2013; Yan *et al*, 2015) is used to specify the wavemaker motion, which provides the wave amplitudes $a_i$, frequencies $\omega_i$ and the phase angles $\varphi_i$ of a list of wave components. In this paper, neither the details of the wave components to specify the wavemaker motion nor the geometry of the wave paddle are given. Furthermore, the geometry of the basin bed is also not flat, except in the working area. Therefore, to reproduce the wave conditions identical to those in the experiment, the self-correction wavemaker (Ma, *et al.*, 2015) is employed in this study. A summary of this technique is given here for completeness. The initial amplitudes and phases of the wave components driving the motion of the wavemaker are given by $a_i^0 = \sqrt{2S(\omega i)\Delta\omega}$ and $\varphi_i{}^0 = k_i x_f - \omega_i t_f$, $i = 1, 2 \ldots N$, where $x_f$ and $t_f$ are the specified focusing location and time, respectively. The target spectrum $S^*(\omega)$ and phase $\varphi^*$ are obtained by applying FFT to the measured surface elevation $\eta^*(t,x_r)$ at a specific gauge location $x_r$ in the experiment. Then iterations are carried out in the following procedures: (i) At the n$^{th}$ iteration, the wavemaker motion is specified by using $a_i{}^n$ and $\varphi_i{}^n$, based on the second order wavemaker theory (Schäffer, 1996), and the surface elevation $\eta^n(t,x_r)$ is recorded; (ii) The amplitude and the phase of each component are corrected by $a_i^{n+1} = a_i^n \sqrt{S^*(\omega i)/S^*(\omega i)}$, $\varphi_i{}^{n+1} = \varphi_i{}^n + \varphi_m{}^*(\omega_i) - \varphi_m{}^n(\omega_i)$, where the subscription $m$ denotes the average phase within the range $[\omega_i - \Delta\omega/2, \omega_i + \Delta\omega/2]$; (iii) The error between $\eta^*(t,x_r)$ and $\eta^n(t,x_r)$ is calculated by using the formula, $Err = \max\{(\eta^* - \eta^n)^2/\eta^{*2}\}$. If $Err$ is sufficiently small, the iteration stops; Otherwise, $n = n + 1$, go to step (i). Although this approach seems to calibrate the wave in the observation point, numerical investigations have indicated that the wavemaker motion specified in such a way result in a satisfactory agreement between the numerical wave elevation with the experimental data at other locations. The effectiveness of this technique has been demonstrated by Ma, *et al.* (2015), and readers can refer this reference for further details. For convenience, this technique is referred to as the self-correction wavemaker technique.

The second approach to numerical wave generation is to specify the boundary conditions at the wave inlet boundaries, including the wave elevation $\eta$, velocity $\vec{u}$ and pressure $p$, using established wave theories, e.g. linear, second-order, Stokes wave theories and stream functions. There are toolboxes, e.g. Jacobsen *et al.* (2011) and Higuera *et al.* (2013), available for such purposes within OpenFOAM. For generating the wave group and/or NewWave, both linear and second order wave theory (Dalzell, 1999) have been attempted in CFD practices (Hu *et al.*, 2014, 2016 and 2017; Yan *et al.*, 2019). For uni-directional waves, the second-order wave elevation, horizontal velocity $u_h$ and vertical velocity $u_v$ can be expressed as,

$$\eta = \sum_{i=1}^{N} A_i cos[k_i x - \omega_i t + \varphi_i] + \eta^{(2)} \quad (12)$$

$$u_h = \sum_{i=1}^{N} \frac{gA_i k_i}{\omega_i} \frac{\cosh(k_i z)}{\cosh(k_i h)} cos[k_i x - \omega_i t + \varphi_i] + u_h^{(2)} \quad (13)$$

$$u_v = \sum_{i=1}^{N} \frac{gA_i k_i}{\omega_i} \frac{\sinh(k_i z)}{\cosh(k_i h)} sin[k_i x - \omega_i t + \varphi_i] + u_v^{(2)} \quad (14)$$

where the superscript (2) denotes the corresponding second order terms, which are detailed by Dalzell (1999) and Hu *et al.* (2014). Ignoring the second order terms, Eqs. (12-14) are downgraded to linear wave theory. Hu *et al.* (2014) compared the linear and second-order wave theory and concluded that the second order terms play an important role for reproducing the focusing wave group in extreme conditions. Therefore, second order theory is used in this paper for the wave generation. Similar to wave generation by using the physical wavemaker, $a_i$, $\omega_i$ and $\varphi_i$ for all wave components at the wave inlet need to be specified *a priori*. An iteration procedure similar to the self-correction mechanism used by Ma, *et al.* (2015) may be used to target the expected wave time histories at a specific location, e.g. the measured data by a wave gauge. It is noted that CFD models using the VOF method need to specify the volume fractions at the computational cells on the wave inlet boundaries, which are not directly given in the wave theories, e.g. Eqs. (12-14). Nevertheless, once the free surface profile is given by the wave elevation, e.g. Eq. (12), the ratio of the volume occupied by the wave over the total volume of the computational cell can be determined. A detailed numerical formulation may be found in Yan and Ma (2010), Jacobsen *et al*.(2011) and Higuera *et al*.(2013). It is also noted that near the wave inlet boundaries, a relaxation zone (Lin & Liu, 1999; Lara *et al*., 2006; Jacobsen *et al*., 2011) may be required to secure the continuity/consistency of the solutions at the inlet boundaries and the surrounding area due to two facts, namely (1) that the reflected waves are expected in the computational domain but are ignored in Eqs. (12-14), which is imposed on the wave inlet boundaries; and (2) that the flow specified by Eqs. (12-14) is assumed to be inviscid/irrotational, which may be different from the flow in the computational domain. In brief, this technique is referred to as the second-order wave inlet technique.

In this work, both techniques are used in the QALE-FEM simulation, whereas in the OpenFOAM simulation, the wave is generated using the second-order wave inlet technique. In addition to the wave generation, another critical issue to secure the expected wave for the WSI is to effectively absorb the undesirable waves at the wave outlet boundaries. Without relevant techniques, the reflected wave from such boundaries would eventually propagate to the structure and alter the wave conditions at the site where the structure is placed. In the OpenFOAM simulation, passive wave absorption using the relaxation zone technique is applied and in the QALE-FEM simulation, the self-adaptive wavemaker theory (Yan *et al*., 2016) is applied for the wave absorption.

## 4. Results and Discussions

### 4.1 Numerical Configuration

In the OpenFOAM simulation, the density and kinematic viscosity are taken as 1000 kg/m$^3$ and $10^{-6}$ Pa/s for the water, 1 kg/m$^3$ and $1.48\times10^{-5}$ Pa/s for the air, respectively. The generalized second-order set up in time integration with backward differencing is used and the time step is specified to secure a maximum Courant number of 0.25. The Normalized Variable Diagram (NVD) differencing scheme GAMMA is applied for all convective term discretisation. The second-order Gauss interpolation scheme is chosen for gradient terms (e.g. pressure), and the Gauss linear corrected scheme is selected for the interpolation of the diffusion terms. An under-relaxation factor of 0.7 is used for all variables (e.g. pressure, velocity) to stabilise the numerical schemes and improve convergence. A Preconditioned Conjugate Gradient (PCG) method (see Hestens and Steifel, 1952) is used for solving linear systems with a local accuracy of $10^{-8}$ for all dependent variables (e.g. fluxes) at each time step. OpenFOAM offers a list of options for turbulence modelling, including classic RANS with $k-\epsilon$ or $k-\omega$ and large-eddy simulation (LES). Since the optimisation of the turbulence modelling is not the focus of the paper and, more importantly, the previous study has revealed an insignificant turbulence effect associated with the interaction between extreme wave and FPSO (e.g. Hu et al, 2016; Ransley et al, 2019; Yan et al, 2019). In this study the standard $k-\epsilon$ model is chosen for the turbulence modelling, and $k$ = 1e-8 and $\varepsilon$ = 1e-11 with $\nu_{turb}$ = 0.009 Pa/s are assigned for initiation. Preliminary tests have indicated that the surface tension effect is neglectable for the cases considered in this paper, but it may be important if a violent wave breaking is involved. In this paper, the surface tension is not considered. A rectangular wave tank is used in the OpenFOAM simulation. The left vertical boundary is specified as the wave inlet, where Eqs. (12-14) are used to specify the volume fraction and the velocity at the water phase (that of the air is set as zero), a zero gradient condition is applied for the pressure. The top boundary and the right vertical boundary are specified with a non-reflecting boundary condition, allowing fluid to leave or entre the computational domain, and a zero-gradient pressure condition. On the surface of the moored FPSO, the moving-wall velocity boundary condition and a zero-gradient pressure condition are imposed. On all other boundaries, the non-slip velocity condition and zero-gradient pressure condition are imposed. The QALE_FEM simulation only considers the water and not the air phase. The density of the water is 1000 kg/m$^3$. The numerical wave tank used by the QALE-FEM is rectangular, the same as the OpenFOAM. On the free surface, the boundary condition is specified by Eq. (5). On the left end of the tank, either a self-correction wavemaker (Eq. (6)) or the second-order wave inlet boundary conditions (Eqs. 12-14) are imposed. On the right end of the tank, a self-adaptive wavemaker with Eq. (6) is utilised to specify the boundary condition. All other boundaries are set as non-slip walls.

### 4.2 Wave Generation

The experiment has been carried out in the wave basin first in the absence of the FPSO. These wave-only results can be used to validate the different techniques to generate and model the propagation of the focusing waves by the QALE-FEM and OpenFOAM. Considering the fact that the wave is uni-directional, both the QALE-FEM and the OpenFOAM use a quasi-3D simulation, in which only one cell is used in the transverse direction ($y$-direction) of the wave

propagation ($x$-direction). The boundary condition imposed on two vertical walls along the wave propagation is assigned to be 'empty' in the OpenFOAM, which reduces the dimension of the simulation from three dimension to two dimension. In the OpenFOAM simulation, the length of the domain is defined as $5\lambda_p$, where $\lambda_p$ is the characteristic wave length (3.31m, see Table1). The relaxation zone near the wave inlet has a length of $\lambda_p$ and that near the wave outlet is $2\lambda_p$. The height of the tank is 3.43m including 2.93m depth below the MWL ($z$ = 0). The vertical size of grid cells is chosen to be relatively coarse near the sea bed, but then becomes finer towards the free surface. A confined region ranging from $z$ = -0.2m to $z$ =0.2m contains the free surface, has a uniform vertical mesh size. In the horizontal direction, the cell size is uniform across the whole domain. At the start of the computation, a cosine ramp function is applied over a wave period to Eqs. (12-14) for the purpose of avoiding impulse-like behaviour and reducing the corresponding undesirable transient waves. The number of wave components $N$ = 25 is used for Eqs (12-14) and the wave amplitude spectra are tuned at the wave inlet boundary of the OpenFOAM simulation. Optimisation of the NWT to determine its length, relaxation zones, the wavemaker motion, as well as grid and time step convergence studies for the case were investigated by Hu *et al.* (2016) for the OpenFOAM simulations. In the present work, the horizontal cell size and the vertical cell size in the confined zone near the free surface are taken as 0.04m and 0.02m, respectively. Such mesh resolutions are also used in the cases with FPSO presented in the rest of the paper. The computational domain used in the QALE-FEM has the same size as the experimental wave basin, i.e. 35m × 15.5m× 2.93m. The vertical mesh size increases from the free surface to the seabed following an exponential growth (Ma *et al.*, 2001), whereas, the mesh size in the horizontal direction is uniform, i.e. 0.05 m according to the corresponding convergence investigation. In the QALE-FEM simulation, the incident waves are generated by using two techniques, i.e. using the self-correction wavemaker aiming to match the wave time histories recorded by a wave gauge located at $x$ =12.391m from the wave paddle in the empty tank test (see Ma *et al.*, 2015 for details), and using the second-order wave inlet aiming to reproduce the wave at the focus point to be consistent with the OpenFOAM results.

Figs. 5 & 6 compare the time histories of the wave elevation recorded at the focus point, $x$ = 13.886 m from the wave paddle, and the corresponding amplitude spectra from numerical and experimental data. The spectra are obtained by using the time histories at the time window $-10s \leq t - t_f \leq 6s$, where $t_f$ is the focus time. The measured maximum wave elevation at the focus location is 0.0718m and 0.1006m for *Hs* =0.077m and *Hs* =0.103m, respectively. It is found that the self-correction wavemaker technique adopted by the QALE-FEM reproduces the incident wave well for both wave conditions, the errors in terms of the maximum crest elevation are 1.8% and 5.6% underestimated compared to the experimental data for *Hs* =0.077 m and *Hs* =0.103 m, respectively; the second-order wave inlet technique used by the OpenFOAM simulation leads to a satisfactory focusing wave for the case with *Hs* =0.077 m (error for maximum crest elevation is 0.1% underestimated) but a less accurate result (8% overestimation of the maximum crest elevation) for the case with higher wave steepness (*Hs*

=0.103 m). Nevertheless, the spectra obtained in the QALE-FEM agree well with the experimental data and clearly closer to those obtained using OpenFOAM. It is also observed that difference between the OpenFOAM results and the QALE-FEM are not caused by the theoretical difference between the NS models and the FNPT, but mainly caused by the method used to generate the incident waves, as evidenced by the agreement in the results between the QALE-FEM with the second-order wave inlet technique (the error for maximum crest elevations are 0.7% under-estimated and 5% over-estimated, respectively, for *Hs* =0.077m and *Hs* =0.103m ) and the OpenFOAM results.

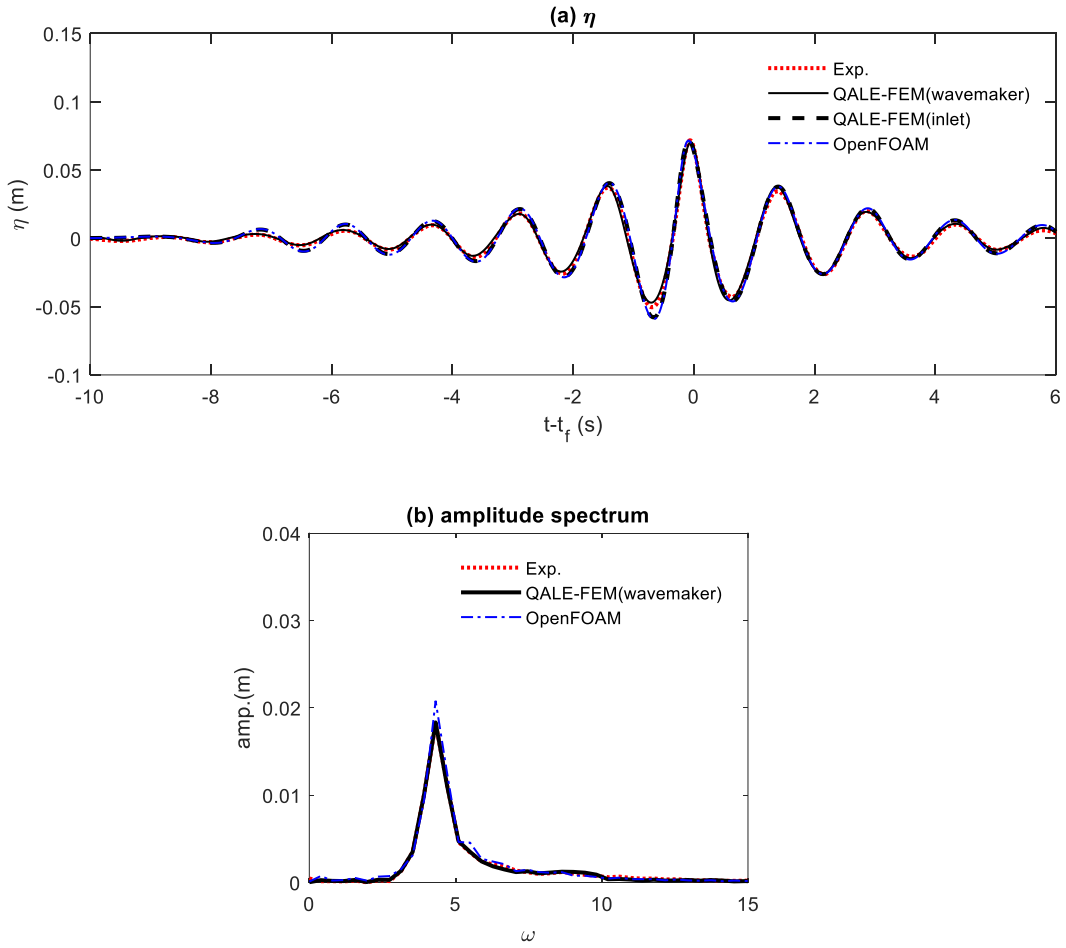


Fig.5 Comparison of (a) surface elevation and (b) amplitude spectrum at focus location (Hs =0.077m; spectra obtained using the data at $-10s \leq t - t_f \leq 6s$; OpenFOAM and QALE-FEM use the 2$^{nd}$ order wave inlet and self-correction wavemaker techniques, respectively)

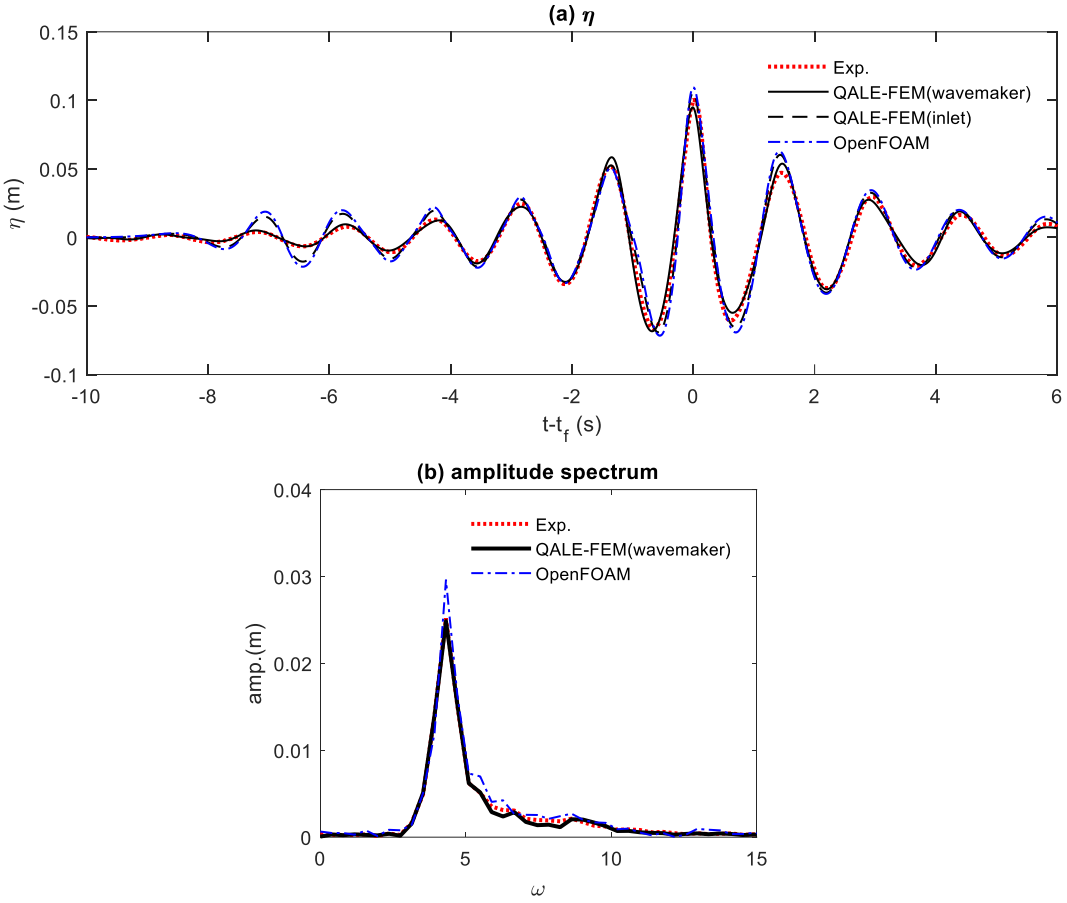


Fig.6 Comparison of (a) surface elevation and (b) amplitude spectrum at focus location ($Hs$ =0.103m; spectra obtained using the data at $-10s \leq t - t_f \leq 6s$; OpenFOAM and QALE-FEM use the second-order wave inlet and self-correction wavemaker techniques, respectively)

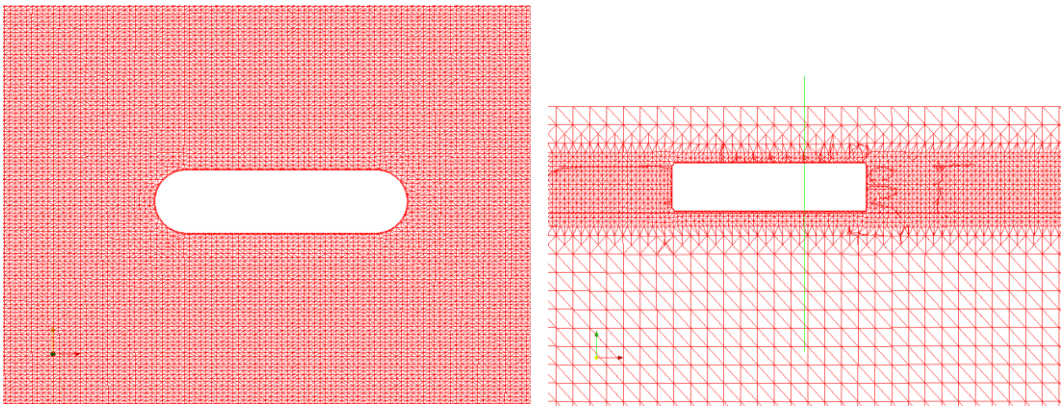

(a) Horizontal section (b) vertical section

Fig.7 Split-hexahedral mesh near the FPSO used in the OpenFOAM simulation

### 4.3 Wave runup and wave load on a fixed FPSO

After assessing the effectiveness and the accuracy of the wave generation using the cases with an empty tank, the wave load on and the response of the moored FPSO in the two wave

conditions described above are compared in order to quantify the roles of wave generation and viscous effects on the overall accuracies of the QALE-FEM and the OpenFOAM. In the experiment, the bow of the FPSO is positioned at the focus location, i.e. $x$ = 13.886m from the wave paddle.

In the OpenFOAM simulation, the width of the domain is taken as 4m and the length/depth of the domain are the same as those used in the empty-tank test. The mesh used by the OpenFOAM is split-hexahedral mesh, which is illustrated in Fig. 7 around the FPSO. The total number of cells is 1,632,742. The confined zone (-0.2 m to 0.2 m), horizontal (0.04 m) and vertical (0.02 m) cell sizes used to generate the mesh are the same as the wave-only cases indicated above. The OpenFOAM simulation was carried out using 32 processors in a High-Performance Computing (HPC) cluster, which is a quad-core 2.56 GHz with 16 Gb RAM. A dynamic time step with a maximum Courant number of 0.25 is applied. The CPU time was 68 hours for the case with $H_s$ =0.077 m and 74 hours for the case with $H_s$ =0.103 m to achieve the results in a physical duration of 18 s.

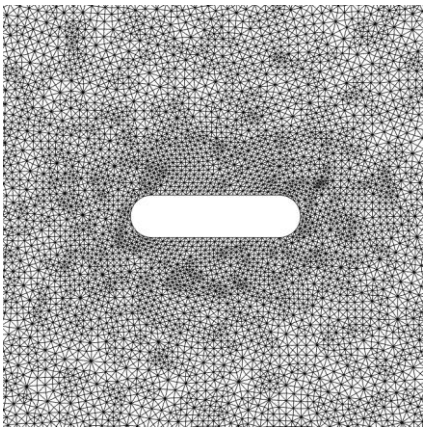

Fig.8 Illustration of unstructured mesh near the FPSO used in the QALE-FEM simulation

The QALE-FEM uses the concept of the overset grid method (Ma *et al.* 2015), in which two sets of computational mesh are used. One covers the entire computational domain (35m × 15.5m× 2.93m) without the FPSO for modelling the nonlinear incident waves. Since the incident wave is unidirectional, the mesh size in the direction normal to the wave propagation can be very coarse, e.g. 4 cells along the transverse direction of the tank. Another one covers a confined zone near the FPSO, i.e. a circular domain with diameter of 7 m centred at the geometric centre of the FPSO. The mesh used in this zone is tetrahedral and is generated by an in-house mesh generator, in which a triangular horizontal mesh, as illustrated in Fig.8, is generated on the free surface and extended vertically towards the seabed. At the outer boundary of the confined zone, the free surface elevation and the fluid velocity are specified by using the solutions from the first set of mesh. A translational zone with a width of 1 m is placed near the outer boundary of the confined zone, in order to damp the reflection from the FPSO. The total number of cells used by the QALE-FEM simulation is 3,449,136. The horizontal mesh size increases from 0.015 m near the FPSO to 0.05 m in the area away from the FPSO. The QALE-

FEM simulations are run in a desktop with Intel Xeon E3-1545 (2.9G) using 4 cores with the OpenMP parallelization. The CPU time is approximately 2 hours for achieving the corresponding results in a duration of 18 s. It is noted that convergence investigations have been carried out for both the OpenFOAM and the QALE-FEM simulation to secure the computational mesh used are sufficient to achieve convergent results.

Compared with the cases with freely-floating FPSO, the cases with a fixed FPSO are ideal to examine the accuracies of the numerical models for wave diffraction and wave loading. Although Ransley *et al.* (2019) and Yan *et al.* (2019) have compared the wave runup and the wave loading on the fixed FPSO in extreme waves and concluded that the overall accuracies of the QALE-FEM and the OpenFOAM are at a similar level, the incident waves generated by the QALE-FEM and the OpenFOAM are different, consequently, it was difficult to quantify the source of the error. In addition to the self-correction wavemaker used by Ransley *et al.* (2019) and Yan *et al.* (2019), herein the QALE-FEM also uses the second-order wave inlet technique to generate the wave, being consistent with the OpenFOAM.

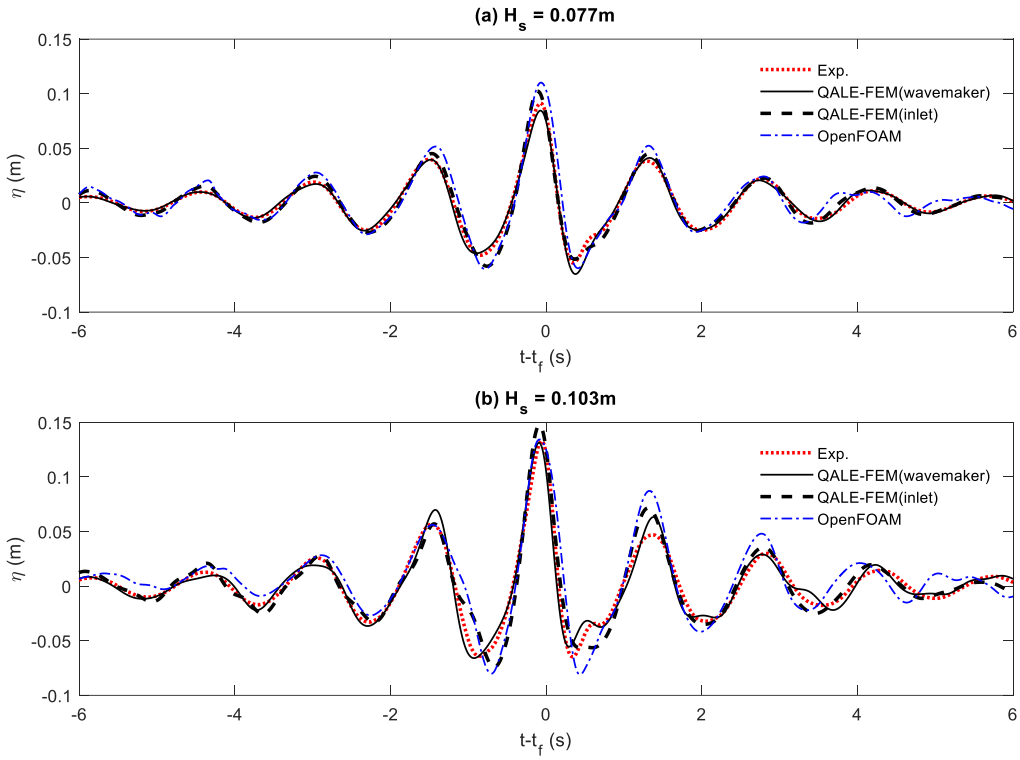


Fig.9 Comparison of the runup at the bow of the fixed FPSO

The time histories of the wave elevation (runup) recorded at the bow of the fixed FPSO (WG16) are compared in Fig. 9. In the case with fixed FPSO, the wave elevation at the bow is expected to be enhanced due to the wave diffraction from the FPSO. The experimental data shows that the peak runup recorded at the bow of the fixed FPSO is 0.0913 m and 0.1331 m, for *Hs* =0.077 m and *Hs* =0.103 m, respectively. It is observed that the QALE-FEM with self-correction wavemaker technique results in numerical results which agree well with the experimental data;

the peak runup recorded at the bow are 0.088 m (relative error -3.6%) for *Hs* = 0.077 m and 0.1314 m (relative error -1.3%) for *Hs* = 0.103 m. The OpenFOAM results over-predict the peak runup at the bow (relative error 20.7%) for $H_s$ = 0.077 m, in which case a similar relative error (16.9%) is observed in the result the QALE-FEM with the second order wave inlet technique. This suggests that the error in the OpenFOAM simulation is mainly caused by the wave generation and the viscous effect plays less important role since the runups predicted by the QALE-FEM and the OpenFOAM are similar when they use the same wave generation technique.

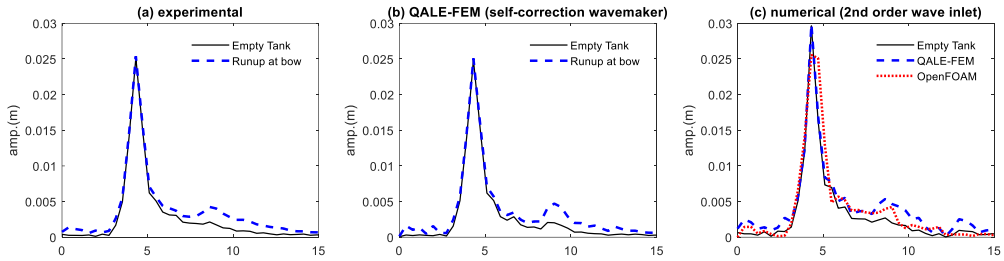


Fig.10 Comparison of the amplitude spectra for (a) experimental results, (b) QALE-FEM results with self-correction wavemaker and (c) numerical results with the second-order wave inlet technique in the cases with *Hs* =0.103 m (spectra obtained using the data at $-10s \leq t - t_f \leq 6s$)

However, it is found that the OpenFOAM result reasonably agrees with the experimental data for *Hs* = 0.103 m in terms of the peak runup with a relative error of 0.9%; whereas using the same wave generation technique, the QALE-FEM overestimates the peak runup by 10.5%. This may suggest that ignoring the viscous effects in the QALE-FEM results in a considerable overestimation of the peak runup and the turbulence model used in the OpenFOAM may overestimate the turbulence viscosity and thus the overall viscous effects, leading to an underestimation of the peak runup enhancement. This is clearer in Fig. 10, which compares the wave spectra at *x* = 13.886 m (corresponding to the surface elevation at the focus point in the empty tank test and the runup at the bow in the case with FPSO) in the cases with *Hs* = 0.103 m. By comparing Fig. 10(a) and (b), it is found that the wave spectra at *x* = 13.886 m obtained by the QALE-FEM with the self-correction wavemaker technique agree well with the experimental data, confirming the observation in Fig.9. However, in the empty tank tests using QALE-FEM, the wave generated by using the second-order wave inlet technique has more significant fundamental (centred at $\omega \approx 4.3$ rad/s) harmonics (Fig.6(b)) compared with that by the self-correction wavemaker and the corresponding experimental result, consequently, the former leads to more significant second order (centred at $\omega \approx 8.6$ rad/s) and third-order (centred at $\omega \approx 12.9$rad/s) response in the cases with FPSO (Fig. 10(b) and (c)). Nevertheless, in the corresponding results with OpenFOAM (Fig.10(c)), the high-frequency harmonics ($\omega >$ 8.6 rad/s) seems to be supressed by the viscous effects. Such high-frequency harmonics are not significant in the cases with *Hs* = 0.077 m and thus the viscous effect plays an insignificant

role, as shown in Fig. 11. This explains the agreement between the QALE-FEM and the OpenFOAM results with the second order wave inlet technique illustrated in Fig.9(a).

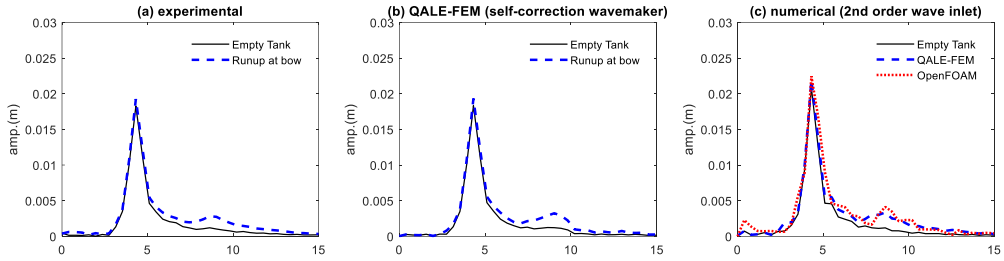


Fig.11 Comparison of the amplitude spectra for (a)experimental results, (b) QALE-FEM results with self-correction wavemaker and (c) numerical results with the second-order wave inlet technique in the cases with *Hs* =0.077m (spectra obtained using the data at $-10s \leq t - t_f \leq 6s$)

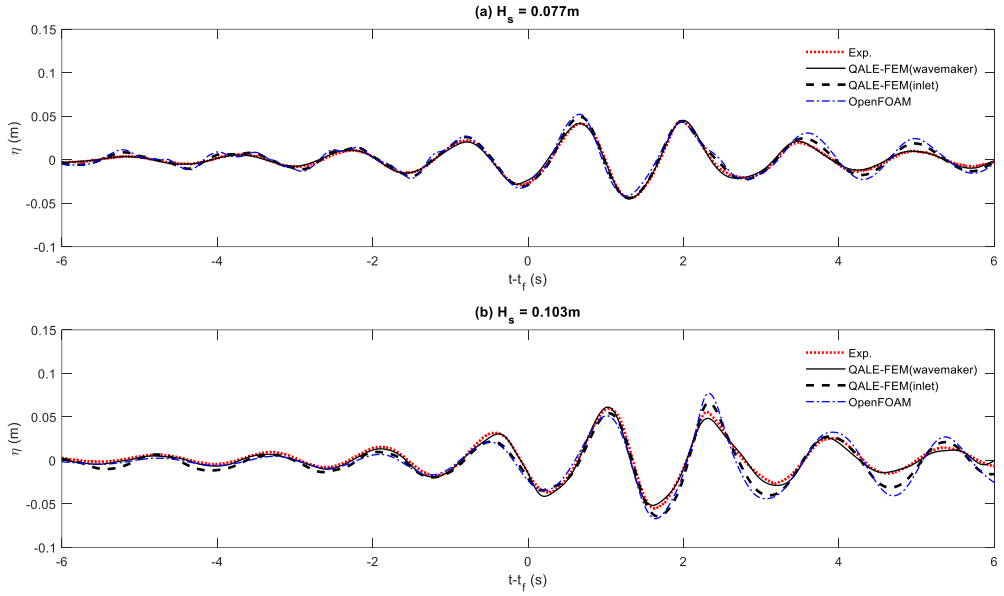


Fig.12 Comparison of the runup at the stern of the fixed FPSO

Compared with the wave elevation (runup) at the bow, that at the stern are insignificant and consequently the viscous effect may be insignificant. As illustrated in Fig. 12, which compares the runup at the stern of the fixed FPSO, the difference between the numerical results and the experimental data is dominated by the wave generation. For the second-order wave inlet technique, both QALE-FEM and OpenFOAM deliver similar numerical results, which are slightly different from the experimental data and the QALE-FEM results with the self-correction wavemaker technique.

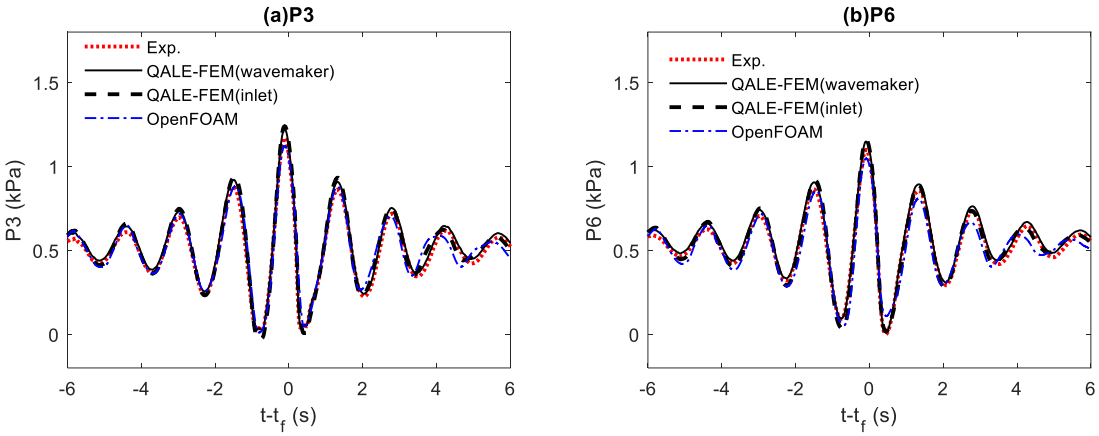


Fig. 13 Comparison of pressure at (a) P3 and (b) P6 in the cases with *Hs* =0.077m

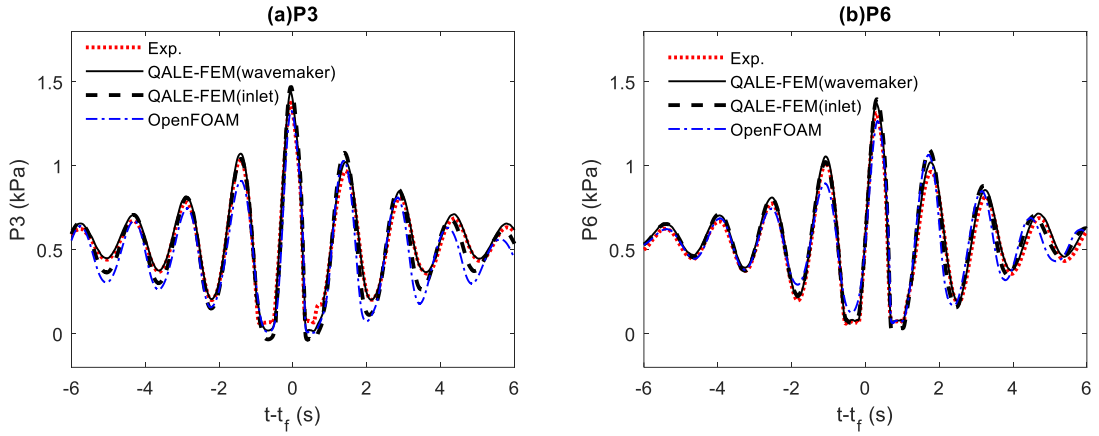


Fig. 14 Comparison of pressure at (a) P3 and (b) P6 in the cases with *Hs* =0.103m

Attention is also paid to the comparisons on the pressure on the surface of the fixed FPSO. Some results recorded at P3 and P6 (see Fig.4), which are located at the 0.05m below the mean water level, are plotted in Fig. 13 and Fig.14 for *Hs* =0.077 m and *Hs* =0.103 m, respectively. Ransley *et al.* (2019) and Yan *et al.* (2019) have shown that the QALE-FEM slightly overestimates the peak pressure on the FPSO surface. This is further confirmed by Fig. 13 and Fig. 14. In the case with *Hs* =0.077 m (Fig. 13), the peak measured pressure is 1.169 kPa at P3 and 1.099 kPa at P6; the QALE-FEM overestimates them by 5% regardless the wave generation technique; whereas the OpenFOAM underestimates the peak pressure by 4% at both pressure sensor locations. As the increase of the wave steepness (Fig. 14 for *Hs* = 0.103 m), the relative error of the QALE-FEM predictions remains similar to those with smaller wave steepness; whereas the OpenFOAM underestimates 3% at P3 and 4% at P6. It is worth noting that, although the error of the OpenFOAM in terms of the peak pressure is lower than the corresponding QALE-FEM simulation, the overall agreement between the QALE-FEM results and the experimental data is good. To quantify the overall agreement, the RMS error defined following Ma and Yan (2005) covering the duration of $-10s \leq t - t_f \leq 6s$ is used. The RMS error of the QALE-FEM with the self-correction wavemaker technique is approximately 5% for all data shown in Figs. 13 and Fig. 14; whereas the RMS error of OpenFOAM is 10% for *Hs* = 0.077 m, 17% and 13% for P3 and P6, respectively, in the cases with *Hs* = 0.103 m. It is also observed that the RMS errors of the QALE-FEM with the second-order wave inlet

technique (i.e. 9% and 15% for *Hs* = 0.077 m and *Hs* = 0.103 m, respectively) are closer to those obtained using OpenFOAM. Once again, it confirms the role of wave generation on securing the accuracy of the WSI modelling.

### 4.4 Motion responses of a moored FPSO in an extreme sea

The motion responses of a moored FPSO in extreme waves are then considered. The geometry and the location of the FPSO considered here is the same as those in the above Section for a fixed FPSO. The mooring configuration in the experiment has been introduced in Section 2. In the OpenFOAM simulation, the mooring line is simplified as a linear spring with a damping coefficient of 0.00001 and a stiffness of 66.3N/m. The centre of gravity of the FPSO is at its water plane centre and 0.07m below the initial water level. The moments of inertia are 1.043, 6.893 and 6.630 N·m·s$^2$ in roll, pitch and yaw, respectively. Using the same HPC cluster as the cases with fixed FPSO, the CPU time to achieve results with a physical duration of 18s is 90 hours and 108 hours for the cases with *Hs* =0.077m and *Hs* =0.103m, respectively. In the QALE-FEM, the same configuration of the mooring system, mass and the moments of inertia as the OpenFOAM are employed, all other parameters are the same as those applied in the cases with a fixed FPSO in the previous section. In addition, an artificial damping ranging from 1.5 - 2.8% of the critical damping may be considered in the motion equation, Eq. (10), of the QALE-FEM simulation to represent the macroscopic effect of the viscosity. The QALE-FEM simulations were run in the same desktop as above using 4 cores with the OpenMP parallelization. The CPU time is approximately 3.6 hours for achieving the corresponding results in a duration of 18s.

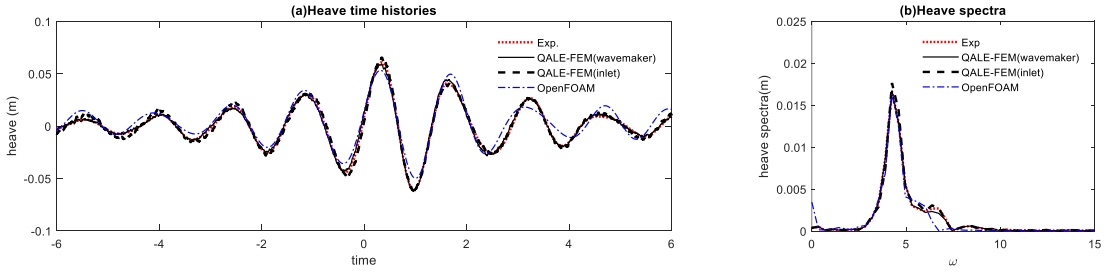


Fig.15 Comparison of (a) heave time and (b) amplitude spectra of the heave motion (*Hs* =0.077m; spectra obtained using the data at $-10s \leq t - t_f \leq 6s$)

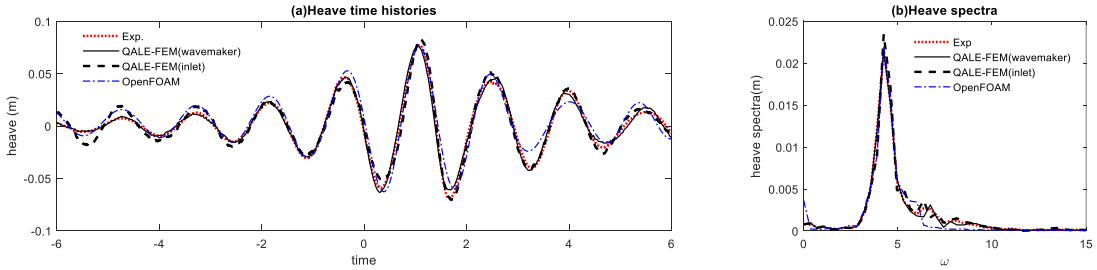


Fig.16 Comparison of (a) heave time and (b) amplitude spectra of the heave motion (*Hs* =0.103m; spectra obtained using the data at $-10s \leq t - t_f \leq 6s$; $[b_t]$=0 and $[b_r] = 0$)

Figs. 15 and 16 compare the time histories of the heave motion and the corresponding motion spectra for *Hs* = 0.077 m and *Hs* = 0.103 m, respectively. As widely accepted, the heave response of the FPSO is largely linear. Good reproduction of the incident wave normally results in a satisfactory prediction of the heave motion. The agreement on the heave time histories between the QALE-FEM results and the experimental data correlates the agreement on the wave elevations shown in Figs. 5 and 6. Typically, the QALE-FEM with the second order wave inlet technique leads to relatively large wave crests before the focusing time, a similar phenomenon is observed in the heave time history, especially in the case with *Hs* =0.103m. The OpenFOAM results behave similarly to the QALE-FEM results with the second order wave inlet boundary condition. The RMS errors covering $-10s \leq t - t_f \leq 6s$ are 8%, 12% and 32% for the QALE-FEM with self-correction wavemaker technique, QALE-FEM with second-order wave inlet and the OpenFOAM in the case with *Hs* = 0.077 m; the corresponding RMS errors are 12%, 22% and 32% in the case with *Hs* = 0.103 m. Nevertheless, the peak values of the heave motions seem to be better predicted. The peak heave motions recorded in the experiment are 0.0608 m and 0.0772 m for *Hs* = 0.077 m and *Hs* = 0.103 m, respectively. In the case with *Hs* = 0.077 m, the corresponding relative error is -2.5%, 8% and -12.5% for the QALE-FEM with self-correction wavemaker technique, QALE-FEM with second-order wave inlet and the OpenFOAM, respectively; the corresponding values are -1%, 7% and -1.8% in the case with *Hs* =0.103m. It is noted that, in the QALE-FEM simulations, the artificial damping coefficients $[b_t]$ and $[b_r]$ in the motion equation are taken as zero. The satisfactory agreement between the QALE-FEM result with self-correction wavemaker and the experimental data suggests that the viscous effect is insignificant in the heave response of the FPSO. The relatively larger error in the OpenFOAM results is not only caused by the effectiveness of the wave generation but also due to the fact that high-frequency ($\omega > 6.3$ rad/s) harmonics are not well captured by the OpenFOAM simulation, being consistent with the observations in the cases with a fixed FPSO.

The time histories of the pitch motions corresponding to Figs. 15 and Fig. 16 are displayed in Fig. 17. It is observed that the QALE-FEM considerably overestimates the pitch motion, although it predicts the heave motion reasonably well. As discussed by Yan and Ma (2007), the viscous effect may play an important role in the rotational motion. An artificial damping coefficient is introduced in the pitch motion, following Yan and Ma (2007). Some results are illustrated in Fig. 18, in which the self-correction wavemaker technique is used. It is clear that by applying an appropriate artificial damping coefficient, i.e. 1.5% critical damping and 2.8% critical damping for *Hs* = 0.077 m and *Hs* = 0.103 m, respectively, the QALE-FEM with self-correction wavemaker technique leads to satisfactory prediction of the pitch motion. However, the coefficients need to be tuned against either experimental data or reliable CFD solutions.

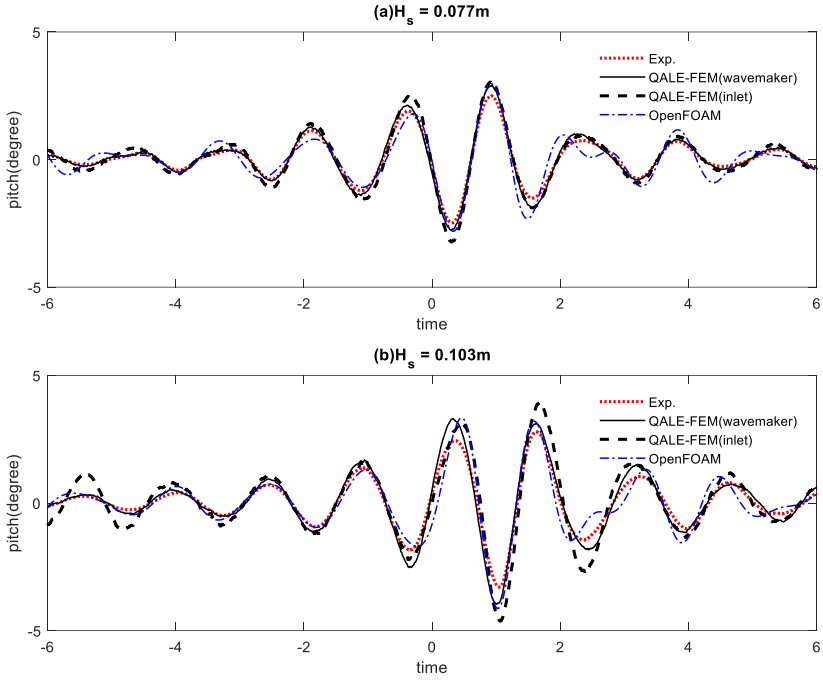


Fig.17 Comparison of time histories of the pitch motions for (a) *Hs* =0.077m and (b) *Hs* =0.103m

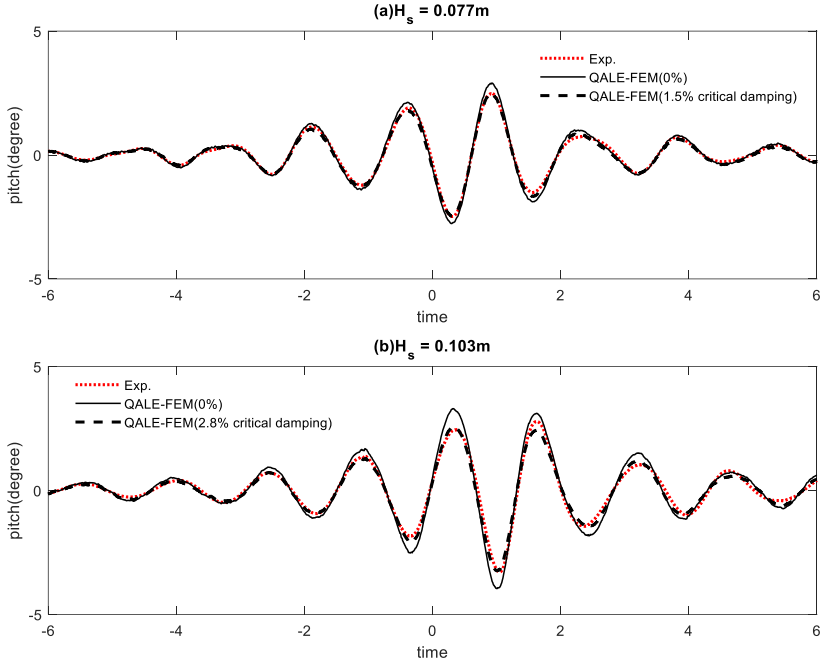


Fig.18 Comparison of time histories of the pitch motions between the QALE-FEM results and the experimental data for (a) *Hs* =0.077m and (b) *Hs* =0.103m (QALE-FEM adopts the self-correction wavemaker technique)

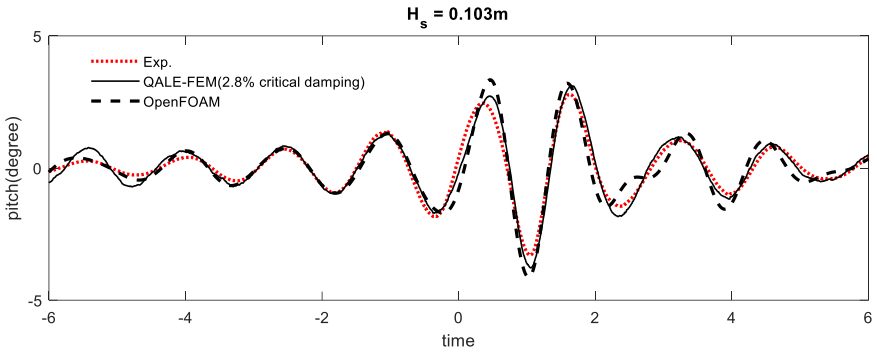


Fig.19 Comparison of time histories of the pitch motions in the cases with *Hs* =0.103m (QALE-FEM adopts second-order wave inlet technique and 2.8% critical damping on the pitch motion)

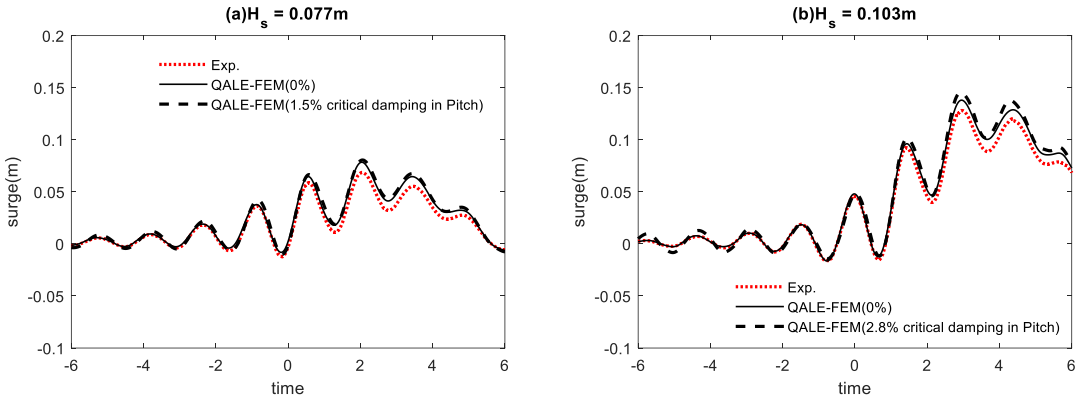


Fig.20 Comparison of time histories of the surge motions (QALE-FEM adopts self-correction wavemaker)

The OpenFOAM simulation has considered the viscous effects in the governing equation, although it may be over-estimated by the selected turbulence model as indicated above. Nevertheless, the OpenFOAM results show an overestimation of the peak pitch motion by 18% and 15% for *Hs* = 0.077 m and *Hs* = 0.103 m, respectively. By using the same technique to generate the incident waves, further comparison is made in Fig. 19 between the OpenFOAM result and the corresponding QALE-FEM with artificial damping. As shown, the OpenFOAM result largely agree with the QALE-FEM result, except that an un-explained high-frequency oscillation exists in the OpenFOAM result after the peak pitch occurs. The reason for this may need to be further explored in the future. Nevertheless, such agreement evidences that the difference between the OpenFOAM result and the experimental results are considerably influenced by the error in the wave generation. It shall be noted that introducing the artificial damping in the pitch motion seems not to significantly influence the QALE-FEM results in other motion modes, as demonstrated by Fig. 20, which compares the time histories of the surge motions between the QALE-FEM results and the experimental data. As observed, the surge motions show a typical feature of low-frequency drift. It is clearer in Fig. 21, which compared the spectra of the surge motion and exhibits a typical dual-peak spectra, one corresponding to the fundamental harmonics centred at $\omega \approx 6.3$ rad/s and the other (more significant) near $\omega \approx 0$. The OpenFOAM seems to overestimate the slow drift (low-frequency harmonics).

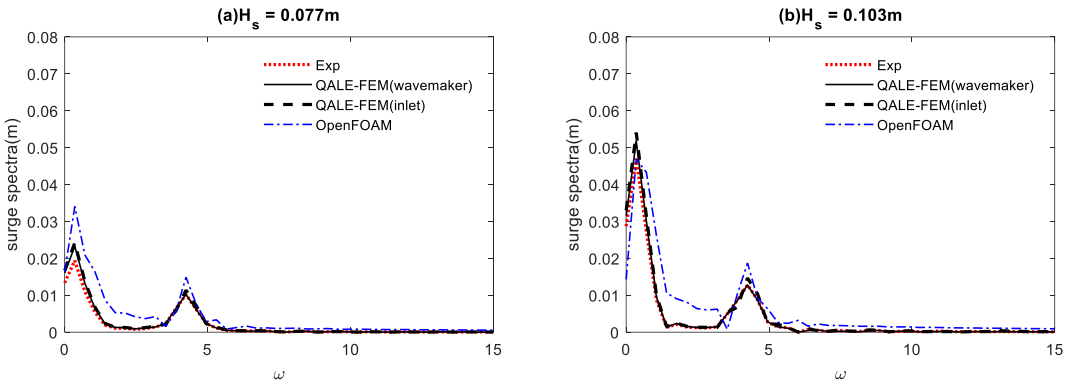


Fig.21 Comparison of amplitude spectra of the surge (spectra obtained using the data at $-10s \leq t - t_f \leq 6s$)

## 5. Conclusions

In this paper, the interaction between extreme waves, generated by focusing NewWave group, and a simplified FPSO is experimentally and numerically studied. Both the two-phase incompressible CFD solver, OpenFOAM, and the FNPT based solver, QALE-FEM, have been applied to the problem. Two approaches to generate the focusing wave, including the self-correction wavemaker theory and the second-order wave inlet technique, are employed. The wave runup and pressure on the FPSO surface, the wave load on and the response of the moored FPSO are examined. By comparing the numerical results with the experimental data, this work aims to (1) quantify the effectiveness of the wave generation technique and its ultimate effects; and (2) shed light on the significance of the viscous effects, on the overall accuracy of the numerical model for WSIs in extreme sea states.

The effectiveness of the wave generation techniques is assessed by comparing predictions of wave only tank tests in which the FPSO is not present. It is concluded that the viscous/turbulent effects are insignificant for the wave generation and propagation considered in this paper, i.e. non-breaking extreme waves, due to the fact that the OpenFOAM and QALE-FEM lead to similar wave time histories at the focus point when using the same wave generation approach. It is also observed that the self-correction wavemaker technique can reproduce the target wave with a satisfactory match on the wave spectra though the peak wave crest may be slightly underestimated, especially the case with high *Hs* = 0.103 m; whereas the second-order wave inlet technique performs better in the case with lower $H_s$ = 0.077 m ).

For simplification and to avoid the influence of the error in the motion response of the FPSO on the related error analysis, the cases with a fixed FPSO are considered for quantifying the main sources of the error on the wave runup and the wave loading. The results reveal that a better reproduction of the incident wave by the self-correction wavemaker generally secures a higher overall accuracy on predicting the wave runup and the wave loading in a non-breaking extreme sea. For the cases with *Hs* = 0.103 m, a considerable viscous effect is identified on wave runup at the bow, where a significant wave enhancement due to the diffraction effect is expected. For both the wave runup and the wave loading, the overall accuracy closely

correlates with the accuracy of the wave generation. The response of the FPSO in extreme waves is examined and results further confirm the correlation between the error in the motion response of the FPSO and that in the wave generation. More importantly, it is concluded that the viscous effect plays an important role in extreme motion response of an FPSO subjected to a focusing wave group, especially in cases with higher *Hs* and an artificial damping coefficient, of 1.5-2.8% of the critical damping, may be necessary to be included in the FNPT model to represent the macroscopic viscous effect on the motion of the FPSO.

Overall, the QALE-FEM can accurately model the wave generation/propagation with high computational efficiency but may fail to achieve a reliable result in the cases with significant wave runup or structure motions (especially the rotational motions) due to its limitation on modelling the viscous effect. In contrast, the two-phase OpenFOAM has capacity of modelling violent wave impact and aeration, can well capture the viscous/turbulence effect, but shows limitation on large-scale wave propagation due to its extensively high computational cost. To take advantages from each and minimise their disadvantages, one may develop a hybrid model combining the QALE-FEM and the OpenFOAM, as suggested by Li *et al* (2018). The present work provides a useful reference for future work aimed at optimising the configuration of the hybrid model to achieve the highest robustness. It is important to note that the conclusions presented here are obtained from cases without wave breaking, aeration and violent wave impact on the FPSO, where the viscous and the turbulent effects are insignificant. Consequently, the conclusions may not be applicable to other cases, such as those involving slamming impact.

## Acknowledgments

The authors would like to acknowledge the supported by the UK Engineering and Physical Sciences Research Council (EPSRC) (Grant number: EP/J012866, EP/J012858, EP/M022382, EP/N006569 and EP/N008863).

## References

Baldock T.E., Swan C., Taylor P.H. 1996. A laboratory study of nonlinear surface waves on water, Proceedings of the Royal Society London, A354, pp 650-675. DOI: 10.1098/rsta.1996.0022.

Brown S., Magar V., Greaves D., Conley D. 2014. Numerical study of turbulent kinetic energy generation under breaking waves. 34th International Conference on Coastal Engineering (ICCE), Seoul, Korea, 15-20 June.

Brown, S, Greaves, D., Magar, V., Conley, D. 2016 Evaluation of turbulence closure models under spilling and plunging breakers in the surf zone, Coastal Engineering, 114, 177-193.

Chen, L.F., Zang, J., Hillis, A.J., Morgan, G.C.J., and Plummer, A.R., 2014. Numerical Investigation of Wave-structure Interaction using OpenFOAM, Ocean Engineering, 88, 91-109.

Dalzell J.F. 1999. A note on finite depth second-order wave-wave interactions, Applied Ocean Research, 21,105-111.

Dias, F, Ghidaglia J, 2018. Slamming: Recent progress in the Evaluation of Impact Pressures, Annual Review of Fluid Mechanics, 50, 243-273.

Ducrozet, G., Bonnefoy, F., Ferrant. P., 2016. HOS-ocean: Open-source solver for nonlinearwaves in open ocean based on High-Order Spectral method. Computer Physics Communications, 10.1016/j.cpc.2016.02.017

Edmund, D.O., Maki, K.J., Beck, R.F., 2013. A velocity-decomposition formulation for the incompressible Navier-Stokes equations, Computational Mechanics, 52, 669–680.

Engsig-Karup, A.P., Eskilsson C. and Bigoni, D., 2016. A Stabilised Nodal Spectral Element Method for Fully Nonlinear Water Waves, Journal of Computational Physics, 318, pp. 1-21.

Fernández H., Schimmels S., Sriram V., 2013. Focused wave generation by means of a self correcting method, Proceedings of the 23rd (2013) International Offshore and Polar Engineering Conference (ISOPE), Anchorage, USA, ISOPE, 3, 917-924,.

Ferrant, P., Gentaz, L., Alessandrini, B., Le Touze, D., 2003. A potential/RANSE approach for regular water wave diffraction about 2D structures, Ship Technology Research, 50, 165–171.

Ferrant, P., Gentaz, L., Monroy, C., Luquet, R., Ducrozet, G., Alessandrini, B., Jacquin, E., Drouet. A., 2008. Recent advances towards the viscous flow simulation of ships manoeuvring in waves, Proceeding of 23rd International Workshop on Water Waves and Floating Bodies, Jeju, Korea.

Fourtakas, G., Stansby, P.K., Rogers, B.D., Lind, S.J., Yan, S. and Ma, Q.W., 2018. On the coupling of incompressible SPH with a finite element potential flow solver for nonlinear free-surface flows. International Journal of Offshore and Polar Engineering, 28(3), pp. 248–254.

Grilli, S.T., Guyenne, P., and Dias, F., 2001. A fully non-linear model for three-dimensional overturning waves over an arbitrary bottom, International Journal for Numerical Methods in Fluids, 35(7), 829-867.

Hestens M. R., Steifel E. 1952. 'Methods of Conjugate Gradients for Solving Linear Systems waves', Jouenal of research of the National Bureau of Standards, 49, 409-436.

Higuera P., Lara J.L., Losada I.J. 2013. Realistic wave generation and active wave absorbtion for Navier-Stokes models, Coastal Engineering, 71, 102-118.

Higuera, P., Buldakov, E., Stagonas, D., 2018. Numerical modelling of wave interaction with an FPSO using a combination of OpenFOAM and Lagrangian models, Proceedings of the 28th International Offshore and Polar Engineering Conference, Sapporo, Japan.

Hildebrandt, A., and Sriram, V., 2014. Pressure distribution and vortex shedding around a cylinder due to a steep wave at the onset of breaking from physical and numerical modeling, Proceedings of the 24th International Offshore and Polar Engineering Conference, Vol.3, 405-410, Busan, Korea.

Hong, S.Y., Kim, K.H., and Chul H.S., 2017. Comparative Study of Water-Impact Problem for Ship Section and Wedge Drops. International Journal of Offshore and Polar Engineering. 27, 123-134.

Hu Z.Z., Causon D.M., Mingham C.M. and Qian L. 2009. Numerical wave tank study of a wave energy converter in heave, Proceedlings 19th ISOPE conference, Osaka, Japan. 383-388.

Hu Z.Z., Causon D.M., Mingham C.G. and Qian L. 2010. Numerical simulation of floating bodies in extreme free surface waves, Proceedings of European Geosciences Union General Assembly (EGU) conference, Vienna, Austria. 12, EGU2010-4927-1, Page:1927

Hu Z.Z., Causon D.M., Mingham C.G. and Qian L. 2011. Numerical Simulation of Floating Bodies in Extreme Free Surface Waves. Journal of Natural Hazzards and Earth System Sciences, 11(2), 519-527

Hu Z.Z., Greaves D., Raby A.2014. Simulation of extreme free surface waves using OpenFoam, 5th Conference on the application of physical modelling to port and coastal protection, Varna, Bulgaria. Vol. 2, pp. 243-252.

Hu Z.Z., Greaves D., Raby A. 2016. Numerical Wave Tank Study of Extreme Waves and Wave-Structure Interaction Using OpenFoam®, Ocean Engineering, 126, pp 329-342.

Hu Z.Z., Mai T., Greaves D., Raby A. 2017. Investigations of Offshore breaking Wave Impacts on a large offshore Structure, Journal of Fluids and Structure, 75, pp 99-116.

Jacobsen N.G., Fuhrman D.R., Fredsøe J. 2011. A wave generation toolbox for the opensource CFD library: OpenFoam, International Journal for Numerical methods in Fluid, 70(9), 1073-1088.

Jasak H., 2007. Automatic mesh motion for the unstructured finite volume method, Transactions of FAMENA, 30(2), 2007.

Jasak, H., 2009. OpenFOAM: Open source CFD in research and industry. International Journal of Naval Architecture & Ocean Engineering, 1(2):89-94.

Johannessen T.B., Swan C. 2001. A laboratory study of the focusing of transient and directionally spread surface water waves, Proceedings of the Royal Society, A457, 971-1006.

Lara J.L., Garcia N, R., Losada, I.J., 2006. RANS modelling applied to random wave interaction with submerged permeable structures. Coastal Engineering 53, 395–417.

Lee, D.H. and Choi, H.S. 2000. A dynamic analysis of FPSO-shuttle tanker system. Proc. 10th Int. Offshore and Polar Eng. Conference, ISOPE, Vol.1, 302-307.

Li, Q, Wang, J.H., Yan, S., Gong, J.Y., Ma Q.W., 2018. A Zonal Hybrid Approach Coupling FNPT with OpenFOAM for Modelling Wave-Structure Interactions with Action of Current, Ocean System Engineering, Vol. 8, pp. 381-407.

Lin, P.Z. and Liu, P., 1999. Internal wave-maker for Navier-stokes equations models. Journal of Waterway, Port, Coastal and Ocean Engineering, 125, 207–215.

Lind, S.J., Xu, R., Stansby, P.K., and Rogers, B.D., 2012. Incompressible Smoothed Particle Hydrodynamics for free surface flows: A generalised diffusion-based algorithm for stability and validations for impulsive flows and propagating waves, Journal of Computational Physics,231,1499-1523.

Lind, S.J., Stansby, P.K., Rogers, B.D., 2016. Incompressible–compressible flows with a transient discontinuous interface using smoothed particle hydrodynamics (SPH), Journal of Computational Physics, 309, 129-147

Luquet, R., Ducrozet, G., Gentaz, L., Ferrant, P., Alessandrini, B., 2007. Applications of the SWENSE Method to seakeeping simulations in irregular waves, Proceeding of the 9th Int. Conf. on Num. Ship Hydro., Ann Arbor, Michigan.

Ma, Q.W., 2005. Meshless local Petrov-Galerkin method for two-dimensional nonlinear water wave problems. Journal of Computational Physics, 205(2), 611-625

Ma, Q.W., 2007. Numerical generation of freak waves using MLPG_R and QALE-FEM methods. CMES - Computer Modeling in Engineering and Sciences, 18(3), 223–234.

Ma Q.W., Wu G.X., Eatock Taylor, R, 2001. Finite element simulation of fully non-linear interaction between vertical cylinders and steep waves. Part 1: Methodology and numerical procedure, International Journal for Numerical Methods in Fluids, 36, 265-285.

Ma Q.W. Yan S., 2006. Quasi ALE finite element method for nonlinear water waves, Journal of Computational Physics, 212, 52-72.

Ma Q.W. Yan S., 2009. QALE-FEM for numerical modelling of non-linear interaction between 3D moored floating bodies and steep waves, International Journal for Numerical Methods in Engineering, 78, 713-756.

Ma Q.W., Yan S., Greaves D., Mai T., Raby A., 2015. Numerical and Experimental Studies of Interaction between FPSO and Focusing Waves, Proc. 25th International Ocean and Polar Engineering Conference, Hawaii, USA, pp. 655-662.

Ning D.Z., Teng B., Eatock Taylor R., Zang J. 2008. Numerical simulation of nonlinear regular and focused waves in an infinite water-depth, Ocean Engineering, 35(8-9), 887-899.

Ning D.Z., Zang J., Liu S.X., Eatock Taylor R.E., Teng B., Taylor P.H. 2009. Free surface and wave kinematics for nonlinear focused wave groups, Ocean Engineering, 36(15-16), 1226-1243.

Qian L., Causon D.M., Mingham C.G., Ingram D.M. 2006. A free-surface capturing method for two fluid flows with moving bodies. Proceedings of the Royal Society A: Mathematical, Physical and Engineering Sciences. 462(2065), 21-42.

Ransley, E., Yan, S., Brown, S., Mai, T., Graham, D., Greaves, D.,Ma, Q., Musiedlak, P.-H., Engsig-Karup, A. P., Eskilsson, C., Li, Q.,Wang, J., Xie, Z., Sriram, V., Stoesser, T., Zhuang, Y., Li, Q., Wan, D., Chen, G., Chen, H., Qian, L., Ma, Z., Causon, D., Mingham, C., Gatin, I., Jasak, H., Vukˇcevi´c, V., Downie, S., Higuera, P., Buldakov, E., Stagonas, D., Chen, Q., Zang, J. 2019. A blind comparative study of focused wave interactions with a fixed FPSO-like structure (CCP-WSI Blind Test Series 1), International Journal of Offshore and Polar Engineering, Vol. 29, pp. 113-128.

Rijas, A.S., Sriram, V., Yan, S, 2019. Variable spaced particle in mesh free method to handle wave-floating body interaction, International Journal for Numerical Methods in Fluids, DIO: 10.1002/fld.4751

Rodi, W., 1980. Turbulence Models and Their Application in Hydraulics – A State-of-the-Art Review, IAHR Publication.

Rusche H., 2002. Computational fluid dynamics of dispersed two-phase flows at high phase fractions, PhD thesis, Imperial College, London.

Schaffer H.A., 1996. Second order wavemaker theory for irregular waves, Ocean Engineering, 23(1), 47-88.

Schwarz, T., 2007. RANS Simulations with One and Six Degrees of Freedom Rigid Body Motions, In: New Results in Numerical and Experimental Fluid Mechanics VI, 96, Seiten 178-185. Springer-Verlag , Berlin, Heidelberg. 15 th STAB/DGLR Symposium, 2006-11-29 2006-12-01, Darmstadt (Germany). ISBN 3-540-74458-4.

Sphaier, S.H., Fernandes,A.C., and Correa,S.H. 2000. Maneuvering model for the FPSO horizontal plane behavior. Proc. 10th Int. Offshore and Polar Eng. Conference, ISOPE, Vol.1, 337-344

Sriram, V., Ma, Q.W., Schlurmann, T., 2014. A hybrid method for modelling two dimensional non-breaking and breaking waves, Journal of Computational Physics, 272, 429–454.

Stansby, P.K., 2013. Coastal Hydrodynamics – present and future, Journal of Hydraulic Research, 51(4), 341-350.

Tahar, A., Kim, M.H., 2003. Hull/mooring/riser coupled dynamic analysis and sensitivity study of a tanker-based FPSO, Applied Ocean Research, 25, 367-382.

Tromans P.S., Anaturk A.R., Hagemeijer P. 1991. A new model for the kinematics of large ocean waves-application as a design wave, Proceedings 1st Inter, Offshore and Polar Engineering Conference, Edinburgh, U.K.

Turnbull M.S., Borthwick A.G.L., Eatock Taylor R. 2003. Numerical wave tank based on a σ-transformed finite element inviscid flow solver, International Journal for Numerical Methods in Fluids, 42. 6, 641-663.

Walker D.A.G., Taylor P.H., Eatock Taylor R. 2004. The shape of large surface waves on the open sea and the Draupner New Year , Applied Ocean Research, 26, 73-83.

Wang, J.H. and Ma, Q.W., 2015. Numerical techniques on improving computational efficiency of spectral boundary integral method. International Journal for Numerical Methods in Engineering, 102(10), 1638–1669.

Wang, J.H., Ma, Q. and Yan, S., 2017. On quantitative errors of two simplified unsteady models for simulating unidirectional nonlinear random waves on large scale in deep sea. Physics of Fluids, 29(6). doi:10.1063/1.4989417.

Wang, J.H., Ma, Q.W., and Yan, S., 2018. A fully nonlinear numerical method for modeling wave–current interactions. Journal of Computational Physics, 369, 173–190.

Wang, J.H., Ma, Q.W., Yan, S. and Qin, H., 2018. Numerical study on the quantitative error of the Korteweg–de Vries equation for modelling random waves on large scale in shallow water. European Journal of Mechanics, B/Fluids, 71, 92–102.

Wang, J.X., Wang J.H., Yan S, Ma, Q.W., Xia, G.H., 2019. An improved passive wave absorber for FNPT-NS solver", submitted to the Twenty-ninth International Ocean and Polar Engineering Conference, Honolulu, Hawaii, USA.

Westphalen J., Greaves D. M., Raby A., Hu Z. Z. , Causon D. M., Mingham C. G., Omidvar P., Stansby P. K., Rogers B. D.. 2014. Investigation of wave-structure interaction using state of the art CFD techniques, Open Journal of Fluid Dynamics, 4(1). 18-43.

Westphalen J., Greaves D.M., Raby A, Williams C.K., Taylor P.H., Hu Z.Z., Omidvar P., Causon D.M., Mingham C.G., Stansby P.K., and Rogers B.D. 2010. Numerical Simulation of Wave Energy Converters using Eulerian and Lagrangian CFD Methods, Proceedings of 20th Internation Socity of Offshore and Polar Engineers (ISOPE) conference. Beijing, China. 731-744 in CFD Issue.

Westphalen J., Greaves D.M., Williams C.K. Zang J. Taylor P.H. 2008. Numerical simulation of extreme free surface waves, Proceedlings 18th Internation Socity of Offshore and Polar Engineers (ISOPE) conference, Vancouver, Canada. July 6-11.

Xie Z. 2012. Numerical study of breaking waves by a two-phase flow model, International Journal of Numerical Methods in Fluids, 70(2), 246–268.

Xie Z. 2013. Two-phase flow modelling of spilling and plunging breaking waves, Applied Mathematical Modelling, 37(6): 3698-3713.

Xie Z. 2015. A two-phase flow model for three-dimensional breaking waves over complex topography, Proceedings of the Royal Society A: Mathematical, Physical and Engineering Sciences, 471, 20150101.

Xing, T., Carrica, P., and Stern, F. ,2008. Computational towing tank procedures for single run curves of resistance and propulsion. Journal of Fluids Engineering, 130(10), 1135-1150.

Yan S., Ma Q.W., 2007. Numerical simulation of fully non-linear interaction between steep waves and 2D floating bodies using the QALE-FEM method. Journal of Computational Physics, 221:666–692.

Yan S., Ma Q.W. 2010a. QALE-FEM for modelling 3D overturning waves, International Journal for Numerical Methods in Fluids, 63, 743-768.

Yan, S., Ma, Q.W., 2010b. Numerical simulation of interaction between wind and 2D freak waves, European Journal of Mechanics B/Fluids, 29, 18–31.

Yan, S., Ma, Q.W., 2017, A hybrid approach coupling MLPG-R with QALE-FEM for modelling fully nonlinear water waves, Proceedings of the 27th International Offshore and Polar Engineering Conference, San Francisco, USA.

Yan S., Ma Q.W., Sriram V., Qian L., Ferrer P.J.M., Schlurmann T., 2015. Numerical and Experimental Studies of Moving Cylinder in Uni-directional Focusing Waves, Proc. 25th International Ocean and Polar Engineering Conference, Hawaii, USA, pp. 711-718.

Yan S., Ma Q.W., Wang J.H., Zhou J.T., 2016. Self-adaptive wave absorbing technique for nonlinear shallow water waves, Proc. ASME 2016 35th International Conference on Ocean, Offshore and Arctic Engineering, Busan, Korea, OMAE2016-54475.

Yan, S., Xie Z.H., Li, Q., Wang, J., Ma, Q.W., Stoesser, T., 2019. Comparative numerical study on focusing wave interaction with FPSO-like structure, International Journal of Offshore and Polar Engineering, Vol. 29, pp. 149-157.

Yang, L., Yang, H., Yan, S., Ma, Q.W., and Bihnam, M., 2016. Comparative study on water impact problem. Proceedings of the International Offshore and Polar Engineering Conference, 2016, 27-34.

Yang, L., Yang, H., Yan, S., and Ma, Q.W. , 2017. Numerical Investigation of Water-Entry Problems Using IBM Method. International Journal of Offshore and Polar Engineering. 27. 1-8

Zang, J., Gibson, R., Taylor, P. H., Eatock Taylor, R. & Swan, C. (2006), 'Second order wave diffraction around a fixed ship - shaped body in unidirectional steep waves', Journal of Offshore Mechanics and Arctic Engineering 128, 10.

Zheng, X., Ma, Q.W., and Duan, WY., 2014. Incompressible SPH method based on Rankine source solution for violent water wave simulation. Journal of Computational Physics, 276, 291-314.

Zhou, J.T., and Ma, Q.W., 2010. MLPG method based on rankine source solution for modelling 3D breaking waves. CMES – Computer Modeling in Engineering and Sciences, 56(2), 179-210.